THE JOURNAL OF PHYSICAL CHEMISTRY A

Article

Cite This: J. Phys. Chem. A 2019, 123, 7470−7485

pubs.acs.org/JPCA

Origins of the Electronic Modulations of Bacterio- and Isobacteriodilactone Regioisomers

Matthew J. Guberman-Pfeffer,* Remy F. Lalisse, Nisansala Hewage, Christian Brückner, and José A. Gascón*

Department of Chemistry, University of Connecticut, Unit 3060, Storrs, Connecticut 06269-3060, United States

Supporting Information

ABSTRACT: Advances in the utilization of porphyrinoids for photomedicine, catalysis, and artificial photosynthesis require a fundamental understanding of the relationships between their molecular connectivity and resulting electronic structures. Herein, we analyze how the replacement of two pyrrolic C_β═C_β bonds of a porphyrin by two lactone (O═C−O) moieties modulates the ground-state thermodynamic stability and electronic structure of the resulting five possible pyrrole-modified porphyrin isomers. We made these determinations based on density functional theory (DFT) and time-dependent DFT computations of the optical spectra of all regioisomers. We also analyzed the computed magnetically induced currents of their aromatic π-systems. All regioisomers adopt the tautomeric state that maximizes aromaticity, whether or not transannular steric strains are incurred. In all isomers, the O═C_β−O_β bonds were found to support a macrocycle diatropic ring current. We attributed this to the delocalization of nonbonding electrons from the ring oxa- and oxo-atoms into the macrocycle. As a consequence of this delocalization, the dilactone regioisomers are as—or even more—aromatic than their hydroporphyrin congeners. The electronic structures follow different trends for the bacteriochlorin- and isobacteriochlorin-type isomers. The presence of either oxo- or oxa-oxygens conjugated with the macrocyclic π-system was found to be the minimal structural requirement for the regioisomers to exhibit distinct electronic properties. Our computational methods and mechanistic insights provide a basis for the systematic exploration of the physicochemical properties of porphyrinoids as a function of the number, relative orientation, and degree of macrocycle-π-conjugation of β-substituents, in general, and for dilactone-based porphyrinic chromophores, in particular.

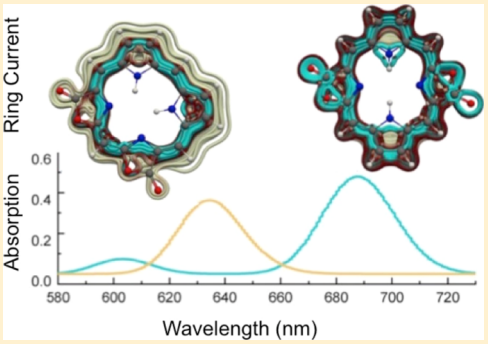

1. INTRODUCTION

Photosynthetic algae, bacteria, and plants universally utilize hydroporphyrins as their key photosynthetic pigments. Algae and higher plants use chlorophylls, Mg(II) complexes of 2,3-dihydroporphyrins (chlorins), whereas phototrophic bacteria employ bacteriochlorophylls, Mg(II) complexes of 2,3,12,13-tetrahydroporphyrins (bacteriochlorins) (Figure 1). Hydroporphyrins are also found in a number of nonphotosynthetic uses. For instance, bonellin, the sex-differentiating green pigment and potent phototoxin to catch prey of a marine green spoon worm, is a free base chlorin.[1] Tunichlorin, a nickel(II) chlorin complex isolated from a Caribbean tunicate,[2,3] is proposed to play a role in reductive processes.[4] Also, prosthetic groups of enzymes involved in multielectron reduction events are 2,3,7,8-tetrahydroporphyrins (isobacteriochlorins).[5,6]

Beyond an adjustment of the oxidation states of the β,β'-bonds within the tetrapyrrolic macrocycle, nature evolved other strategies for tailoring the electronic properties of the tetrapyrrolic chromophores to adapt them to diverse environmental constraints, such as the quantity and quality of the available light or the particular function of the cofactor.[7,8] In general, the physicochemical properties of the (hydro)-porphyrins are modulated through intrinsic electronic and conformational substituent effects,[7−13] as well as the steric and electrostatic contours of their local protein environment.[14]

One particularly potent auxochrome is the carbonyl group, either when established at a benzylic position to the π-aromatic chromophore or when directly attached to the tetrapyrrolic framework (Figure 2).[15] Notably, the specific position of the auxochrome on the chromophore is important, as the differences in the optical properties of the two chlorophylls, *f* and *d* indicate.[16] β-Carbonyl functionalities are also found in nature. One example carrying two β-carbonyl functionalities on adjacent pyrrolic moieties is heme d_1, the prosthetic group of bacterial nitrous oxide, sulfite, and nitrite reductase.[17−20] An example with two β-carbonyl functionalities on opposite pyrrolic building blocks is represented by the family of tolyporphins, green tetrapyrrolic pigments of unknown function isolated from a cyanobacterium-microbial ecological unit.[21−26]

Received: June 13, 2019
Revised: July 29, 2019
Published: July 30, 2019

DOI: 10.1021/acs.jpca.9b05656
J. Phys. Chem. A 2019, 123, 7470−7485

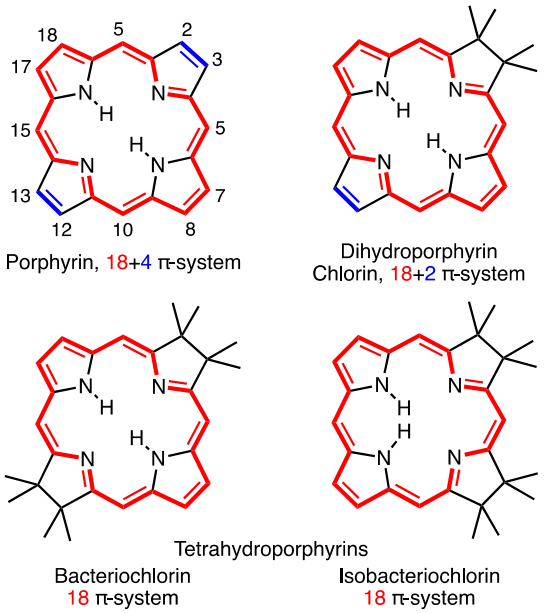

Figure 1. Framework and π-system structures of porphyrin and hydroporphyrin classes, and the numbering system used. Conjugated 18 π-systems highlighted in red, cross-conjugated double bonds in blue.

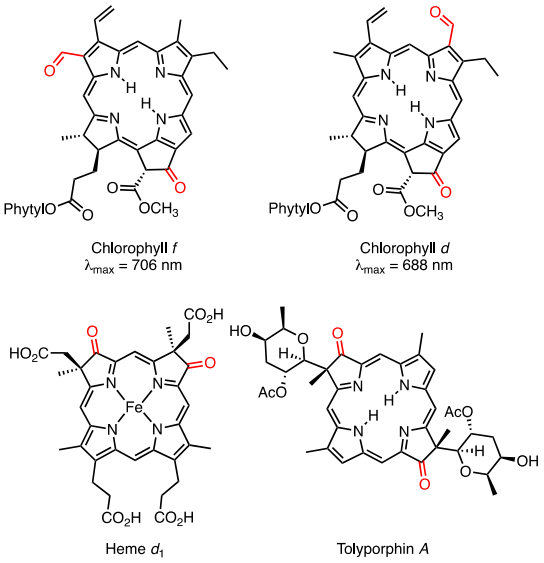

Figure 2. Examples of natural tetrapyrrolic products containing auxochromic carbonyl groups located either in a benzylic position to the chlorin π-system (chlorophylls *f* and *d*) or directly attached to the isobacteriochlorin- (heme d_1) or bacteriochlorin-type π-system (tolyporphin *A*).

An understanding of the operational principles of the electronic (optical) engineering of the porphyrinic chromophore will advance the rational design of synthetic photonic technologies for the purpose of solar energy conversion, small molecule activation, or biomedical diagnosis or therapy. It therefore does not surprise that the synthesis of tetrapyrrolic model systems incorporating β-carbonyl groups has been actively pursued.[10−13,27,28] Particularly, the hydroporphyrin total syntheses and macrocycle modification strategies developed by Lindsey and co-workers allowed the preparation of a wide variety of chromophores carrying carbonyl group-based auxochromes in many different configurations.[11,13] These compounds proved to be of great utility for the fundamental understanding of the electronic structures of these chromophores, as well as of practical utility in medical and technical applications.[11,13]

To the suite of methodologies for the modulation of the optical properties of hydroporphyrins has been added the formal replacement of one or two pyrrolic subunits by non-pyrrolic heterocycles of different ring sizes and compositions.[29−34] A particularly interesting group among these so-called pyrrole-modified porphyrins is the porpholactone family that features the replacement of one or two pyrrolic building blocks by oxazolones.[16,35−39] Thus, one or two β,β-double bonds (HC═CH) of a porphyrin or, from an alternative point of view, one or more β,β-single bonds (H_2C-CH_2) of a hydroporphyrin, were replaced by lactone (O═C−O) moieties, thereby establishing a β-carbonyl group onto the tetrapyrrolic framework. A number of complementary direct and step-wise conversions of *meso*-C_6F_5-porphyrin to porpholactone **0E00** and all five isomeric dilactones have become known (Scheme 1).[16,36,39] For a note on the nomenclature convention for the mono- and dilactones used here, see below.

Porpholactones, as their free bases or metal complexes, found uses as model compounds for naturally occurring prosthetic groups,[16,40,41] as small molecule activation catalysts,[42−44] photocatalysts for oxidative C−H functionalization,[45] or electrocatalysts for the electrochemical evolution of hydrogen.[46] Their optical properties are explored as lanthanide sensitizers,[47] as a component in pressure-sensitive paints,[48−50] as bioimaging and photochemotherapeutic agents,[47,51] or as optical chemosensors.[52−54] The optical properties of porpholactone **0E00** are porphyrin-like, but the properties of its metal complexes are metallochlorin-like.[36,37] The lactone carbonyl group retains strong electronic conjugation with the macrocyclic chromophore, presumably through the retention of an sp^2-hybridized β-carbon atom; consequently, the reduction of the carbonyl group to a hemiacetal (CH(OH)−O) or an ether (CH_2−O) moiety is strongly reflected in the optical properties of the resulting oxazolochlorin-type chromophores.[37,55−59] Zhang and co-workers have shown that the relative orientation of the β-substituents strongly modulates the optical properties in the bacteriodilactone series (**0E0∃** vs **0E0E**);[16] in turn, we were able to demonstrate this for the isobacteriodilactone series (**0E∃0** vs **0EE0** vs **0∃E0**).[39]

However, neither the exact nature of the electronic interaction of the lactone moiety with the macrocyclic π-system, nor its role in the structural origin of the aromaticity or wavelength modulation of the dilactone isomers are fully understood, even though the spectra could be successfully modeled using time-dependent density functional theory (TD-DFT) calculations.[16,39] Likewise, conflicts in the parallels drawn between the auxochromic effects of the carbonyl groups in the bacteriodilactones and the chlorophylls were left unresolved.[16] Most recently, the groups of Shen, Sessler, and Zhang reported on sets of regioisomeric bacteriodilactone-based derivatives of varying degrees of reduction and found that the differences in the optical properties of the regioisomeric pairs were related to the energy level splitting of the frontier molecular orbitals, that the number of saturated subunits within the macrocycle enhanced their regioisomeric differences, and that the difference in the degrees of aromaticity between the regioisomers was also correlated with the magnitude of the regioisomeric effect.[59]

DOI: 10.1021/acs.jpca.9b05656
J. Phys. Chem. A 2019, 123, 7470−7485

Scheme 1. Known Single-Step Syntheses of Porpholactone and All Its Isomeric Dilactones[16,36,39]

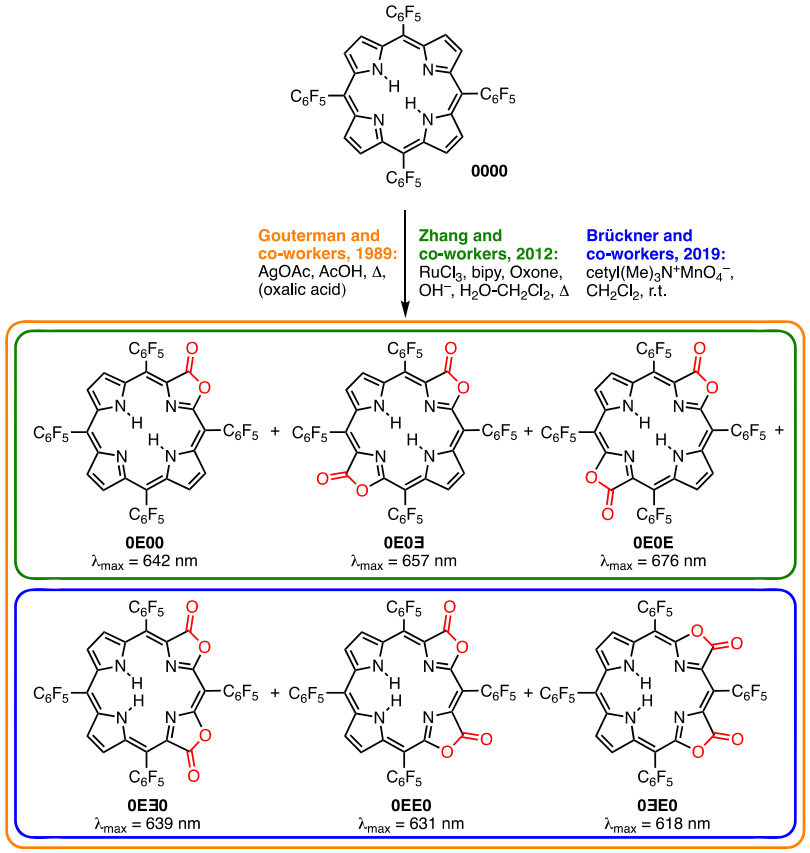

Using the five-compound series of porphodilactone isomers that have recently become available,[16,39] this contribution expands on previous work that demonstrated the strong electronic influence of one[36,37] or two[16,39] lactone moieties on the electronic structure of the chromophore by elucidating in detail the origins of the regioisomeric-dependent optical and magnetic response properties. We previously characterized, without mechanistic detail, some of the thermodynamic and electronic structure properties presented in this study.[39] The present contribution highlights the extent to which the porpholactone isomers behave like regular bacteriochlorins or isobacteriochlorins and where they are subject to unique effects. Moreover, we investigate the interplay of steric and electronic factors within these molecules that determine their thermodynamic stability, including the rotational itinerary of the *meso*-C_6F_5 groups, the conformation of the macrocycle, and their preferred tautomeric state. We also visualize and quantify the aromatic ring currents in the porphodilactones. Importantly, we find that the generalizations derived by the Shen, Sessler, and Zhang article with respect to regioisomeric effects are only valid for certain derivatives that include the porpholactones, but that are not truly general; we also do not find a correlation between aromaticity and the regioisomeric effects.[59]

2. COMPUTATIONAL DETAILS

All structures were optimized at the B3LYP-D3/6-31G(d) level of theory[60−62] and confirmed to be local minima via a vibrational analysis (i.e., no imaginary frequencies). Although the B3LYP functional is commonly used to study porphyrins, previous investigations have found that the relatively small fraction of Hartree−Fock exchange in the functional can result in exaggerated extents of delocalization in annulenes[63−65] and expanded porphyrins.[66,67] For some porphyrinoids,[68] however, B3LYP has been found to provide optimized structures that are comparable to those obtained with the M06-2x functional,[69] which includes more than double the contribution from the Hartree−Fock exchange as B3LYP.

To assess the structural relevance of the chosen functional for the present article, geometry optimizations and vibrational analyses were also performed for the regioisomeric porphodilactones at the CAM-B3LYP-D3/6-31G(d) level of theory.[70] The maximal differences in bond lengths and angles for all five isomers were ≤0.02 Å and 1.0°, respectively. As these structural changes are likely within the intrinsic error of either density functional approximation, any geometric correction to over-delocalization offered by CAM-B3LYP for this series of compounds seems to be minimal. The B3LYP-optimized structures were therefore used for our analyses unless otherwise noted.

Excitation energies were simulated with TD-DFT using the PBE0[71] functional with a 6-31+G(d) basis set. This functional was chosen after extensive testing against CAM-B3LYP, as detailed in the Supporting Information. Whenever the effect of implicit CH_2Cl_2 solvation was assessed, the conductor-like polarizable continuum model was used for structure optimization and spectral simulation.[72,73]

A constant shift was applied to all calculated excitation energies to align the simulated Q_y absorption maximum with the experimental band for the parent porpholactone **0E00**. The required shift was 0.24 eV for structures with *meso*-C_6F_5 groups in implicit CH_2Cl_2 solvent, which increased by 0.12 eV when

DOI: 10.1021/acs.jpca.9b05656
J. Phys. Chem. A 2019, 123, 7470−7485

hydrogen atoms replaced the *meso*-aryl groups and the calculations were instead performed in vacuum. These errors are reasonable for TD-DFT,[74] and as shown in the Supporting Information, the chosen model chemistry is qualitatively quite reliable.

NMR calculations were performed using the GIAO method[75−78] with the B3LYP/def2TZVP[79] model chemistry. The basis set and perturbed densities from these calculations were analyzed with the gauge including magnetically induced current (GIMIC) method[80,81] to visualize ring current pathways and to quantify current susceptibility strengths. The model chemistry used for the NMR calculations has been recommended for the study of diatropic porphyrinoids using GIMIC.[68,82] We have nonetheless assessed the potential of B3LYP to exaggerate delocalization[83−85] and thereby overestimate aromaticity by also performing the ring current analysis for the regioisomeric porphodilactones using either B3LYP or CAM-B3LYP on the structures optimized with CAM-B3LYPY. The trends in current susceptibility were found to be invariant to the use of either exchange−correlation functional for the geometry optimizations, current susceptibility calculations, or both (see the Supporting Information for details).

The current susceptibilities were quantified by integrating the current density passing each symmetry nonequivalent nitrogen atom and β,β-bond (C═C or C−O), as well as one $C_\alpha-C_{meso}$-bond. The sum of the currents through the nitrogen atom and $C_\beta-C_\beta$ or $C_\beta-O_\beta$ bond of each subunit matched the current through the $C_\alpha-C_{meso}$-bond to within 0.7 nA/T. This minor numerical deviation from Kirchhoff's current law is due to the numerical approximation to the integration planes, and the placement of some of these planes through nitrogen atoms, which sustain local currents. The discrepancy is reasonably small and does not alter the conclusions.

In separate NMR calculations, a probe atom was placed 1.0 Å above the geometric mean of the $C_{12}N_4$ inner macrocycle common to all studied molecules to determine the nucleus-independent chemical shift (NICS) for the macrocycle.[86,87] The negative of the ZZ component of the magnetic shielding tensor calculated at this position is reported in the text as $NICS(1)_{ZZ,macro}$.

All structure optimizations, vibrational analyses, excitation energies, and NMR properties were calculated with an ultrafine integration grid for DFT or TD-DFT as implemented in Gaussian 09 Revision D.01.[88]

3. RESULTS AND DISCUSSION

3.1. Structural Considerations and Nomenclature. Conversion of two pyrrole subunits of a porphyrin into oxazolone moieties yields five possible isomeric porphodilactones (Scheme 1).[16,36,39] Two of the regioisomers display oxazolones on opposite sides of the macrocycle, resembling the substituent pattern of bacteriochlorins. The other three isomers resemble isobacteriochlorins, with oxazolones at adjacent sites. The naming as (iso)bacteriochlorins is purely based on structural considerations and does not imply that these chromophores possess bacteriochlorin- or isobacteriochlorin-like optical properties. We will show below that they, in fact, do not.

In the bacteriochlorin series, the two lactone moieties can adopt two relative orientations:[16,36,39] head-to-tail (2,12-dioxa-3,13-dioxo-substitution, C_{2h}-symmetric structure) and head-to-head (2,13-dioxa-3,12-dioxo-substitution, C_{2v}-symmetric structure). For the purpose of the symmetry assignments, the relative orientation of the *meso*-C_6F_5-groups with respect to the chromophore mean plane is ignored. Three orientations are possible in the isobacteriochlorin series: head-to-tail (2,7-dioxa-3,8-dioxoporphyrins), head-to-head (2,8-dioxa-3,7-dioxoporphyrins), and tail-to-tail (3,8-dioxa-2,7-dioxoporphyrins).

The formal numbering system,[89] however, is not particularly user-friendly and does not provide any direct indication of the symmetry of the molecule. We therefore introduce here a nomenclature convention using a four-character string representing the building blocks in a way that specifies the position and relative orientation of the oxazolones, and that allows a rapid survey over the (relative) symmetry of the molecules: a pyrrole moiety is designated **0**, for example, a regular (*meso*-aryl)-porphyrin is named **0000**. A lactone moiety is designated **E** in one orientation and **∃** in the opposite orientation. Thus, a porphomonolactone is named **0E00**. For convenience, we chose to start the string for the chromophores in the orientation shown in Scheme 1 at the top-left ring and then enumerate in clockwise fashion. Going around a macrocycle, the last character in the string is followed by the first again, so the monolactone could equivalently be named **00E0** or **000E**, and so forth (or even **∃000**, etc., as the compound is nonchiral).

Two lactone moieties within a macrocycle can be adjacent (isobacteriochlorin-type substitution), such as **0EE0**, or opposite (bacteriochlorin-type substitution, i.e., separated by a pyrrole) from each other, as in **0E0E**. Both lactones could also be arranged in the same orientation (head-to-tail) in the macrocycle (EE) or opposite (head-to-head) (∃E) to each other. When comparing multiple structures, it is important to construct the string by traversing the macrocycles in the same clockwise or counterclockwise direction, regardless of where the string was started. Therefore, the two bacteriodilactone isomers are **0E0E** and **0∃0E** when starting the string with the top-left pyrrole, but other strings are equivalently valid. Likewise, the isobacteriodilactone isomers are designated as **0E∃0** (tail-to-tail; C_{2v}-symmetry), **0EE0** (head-to-tail; C_s-symmetry), and **0∃E0** (head-to-head; C_{2v}-symmetry). Thus, some structural information and symmetry elements of the molecules are directly reflected in the character strings. We see this as the greatest advantage of the proposed system. We also note that this nomenclature can be expanded to tetrapyrrolic macrocycles containing more than two lactones (such as **EEE0**), smaller (**0E0** for Osuka's subporpholactone, for example)[90] or larger number of "pyrroles" within the macrocycles (**E0000** for a hypothetical pentaphyrin lactone), and, using additional characters, to macrocycles containing other non-pyrrolic moieties.

In theory, there are multiple tautomeric structures available to the dibasic chromophores discussed here. We refer to tautomeric structures carrying two N−H protons at adjacent sites as *adj*-isomers and those carrying them at opposite sites as *opp*-isomers. In case of the porpholactones, some of the tautomeric possibilities position N−H hydrogen atoms on oxazolone moieties. However, computations presented below will show in detail that all tautomers carrying N−H hydrogen atoms on the oxazolones are much disfavored. They were therefore not specifically named.

3.2. Macrocycle and *meso*-Aryl Conformational Effects. Single crystal X-ray diffractometry structures of the *meso*-C_6F_5−porphodilactone isomers, as their free bases or zinc(II) complexes, are available and demonstrate that their

DOI: 10.1021/acs.jpca.9b05656
J. Phys. Chem. A 2019, 123, 7470−7485

chromophores are all idealized planar.[16,39] The optimized geometries of the free base bacteriodilactones and isobacteriodilactones presented here are qualitatively consistent with the experimental findings: the structures are essentially planar, with only a minor tilt (up to 4°) of the O=C−O moiety of each oxazolone from coplanarity with the $C_{16}N_4$ macrocycle. The minor oxazolone out-of-plane distortion was previously attributed to an unfavorable steric interaction between the carbonyl and a flanking *meso*-C_6F_5 group.[37,91] Evidently, the steric repulsion is greater than the electrostatic attraction that could be expected to exist between the negatively polarized oxygen terminus of the carbonyl and the partial positive π-face of the C_6F_5-ring.

The carbonyl−*meso*-aryl steric repulsion responsible for the oxazolone out-of-plane deformation should directly correlate to the distance between these two groups, which itself is dependent on the tilt angle of the C_6F_5-ring. To explore the nature and energetics of this interaction, relaxed potential energy surface (PES) scans were conducted around the C_{meso}−C_{ipso} bond of the symmetry-unique C_6F_5-groups in **0E0∃** and **0E0E** (see the Supporting Information), as well as the C_6F_5-groups flanked by two, albeit differently oriented, oxazolones in **0E∃0**, **0EE0**, and **0∃E0** (Figure 3). The *meso*-C_6F_5 groups of the fully optimized structures are rotated by 17−30° off orthogonality to the plane of the macrocycle.

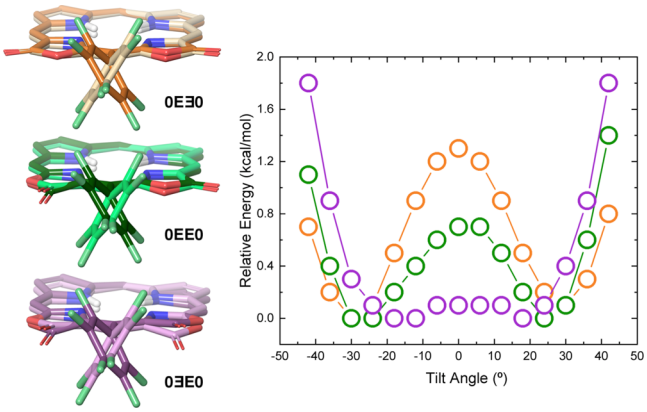

Figure 3. Structures (left) and corresponding energetics (right) for the rotational itinerary (±42° off-orthogonality) of the *meso*-C_6F_5 group in-between the two oxazolones of the isobacteriodilactone isomers shown. The overlaid light and shaded structures are the initial and final geometries from the PES scans, respectively.

There is competition between the preference for a tilted, as coplanar as possible *meso*-C_6F_5 ring to realize (partial) conjugation with the macrocyclic π-system,[92] and a steric clash between the *o*-F atom and the lactone carbonyl group that develops as the ring tilts and induces an out-of-plane distortion of the oxazolone.[37,91] The PES results allow an assessment of the relative energies of both effects.

The competition between the steric and electronic effects is most clearly evident in the comparison of the PES scans conducted for the isobacteriodilactone isomers, **0E∃0** and **0∃E0**, which respectively have no or two steric clashes between the aryl and carbonyl groups. In the absence of the steric interactions, the perfectly orthogonal orientation of the *meso*-aryl group is ∼1.3 kcal/mol less favorable than a ∼30° tilt angle (the energy minimum in the PES). The destabilization reflects the loss of (partial) conjugation of the aryl substituent with the macrocycle. In contrast, the rotational itinerary for the isomer with two steric interactions is energy-neutral in the tilt angle range between ±20° because the stabilization provided by conjugation to the macrocycle as the C_6F_5-ring tilts is now opposed by steric contacts with the oxazolone carbonyls. Isomer **0EE0** with only one of these interactions takes up a middle position between the limiting cases. Comparison of the rotational barrier height at a 0° tilt for **0∃E0** to **0EE0** and **0EE0** to **0E∃0** shows that each successive carbonyl−*meso*-aryl steric repulsion destabilizes the structure by an additional ∼0.7 kcal/mol.

These observations also apply to the bacteriodilactones (for details, see the Supporting Information). The rotational itinerary of the C_6F_5-group in the bacteriodilactones on the oxa-side of the oxazolone (interaction of the *o*-F with the β-O and CH groups) compares to the interaction of the *o*-F with the two β-O groups in **0E∃0**. Likewise, the itinerary for the aryl group on the oxo-side of the oxazolone in the bacteriodilactones is equivalent to that shown for **0EE0**.

Given the energetically small (<1.5 kcal/mol) steric and conjugation effects, we emphasize that the relative magnitudes are more important than their absolute values. We therefore conclude from the forgoing discussion that the conjugation effect and the steric interactions with two carbonyl groups are of the same magnitude in the rotational space ± 35° off-orthogonality; beyond this range, steric interactions overcome all conjugation effects.[92] We will demonstrate below that the *trends* in the thermodynamic and spectral properties of the porphodilactones are largely unaffected by the presence of the *meso*-C_6F_5 groups, even though the absolute values shift with their presence.

3.3. Ground-State Stability. The thermodynamic stability of the most stable tautomers of the porphodilactone isomers (*opp*-bacteriodilactone and *adj*-isobacteriodilactone isomers; see below for details) depends on the relative orientation of the oxazolone subunits, with the most stable being the bacteriodilactone **0E0∃**, followed by the other bacteriochlorin-type isomer **0E0E** (Table 1); the least stable and experimentally also most rare[39] isobacteriodilactone is isomer **0∃E0**. Overall, the stability rank ordering is **0∃E0** < **0EE0** < **0E∃0** ≪ **0E0E** < **0E0∃**. Any of the three isobacteriodilactones are disfavored by 7−9 kcal/mol relative to either of the bacteriodilactones. In comparison, the parent unsubstituted isobacteriochlorin is only ∼4 kcal/mol less stable than the corresponding unsubstituted bacteriochlorin.

Table 1. Relative Total Energies (kcal/mol) for Isomeric Dilactones and Reference Structures[a]

structure	with C_6F_5, in CH_2Cl_2	without C_6F_5, in CH_2Cl_2	with C_6F_5, vacuum	without C_6F_5, vacuum
0E0∃	0.0	0.0	0.0	0.0
0E0E	0.6	0.5	0.5	0.5
0E∃0	6.1	7.0	6.9	7.6
0EE0	7.1	7.4	8.0	8.1
0∃E0	8.6	8.3	10.0	9.3
bacteriochlorin				0.0
isobacteriochlorin				3.9

[a]Relative energies for the structures optimized at the B3LYP-D3/6-31G(d) level of theory. Calculations including solvent used the conductor-like polarizable continuum model.

DOI: 10.1021/acs.jpca.9b05656
J. Phys. Chem. A 2019, 123, 7470−7485

This stability order is the same, irrespective of the replacement of the *meso*-C_6F_5 substituents by hydrogen atoms, or whether implicit CH_2Cl_2 solvation is included or not in the computations. For simplicity sake, we therefore focused on vacuum-optimized chromophore structures carrying *meso*-hydrogen atoms. We also compare molecular electronic energies only because entropic differences among the isomers are likely to be minimal.[93]

3.4. Tautomeric Preferences of the Porphodilactone Isomers. The investigation of porphyrin and hydroporphyrin tautomers, and their analogues, has a long history.[94−102] The preferred tautomer for porphyrins, chlorins, and bacteriochlorins is the *opp*-tautomer, whereas the isobacteriochlorins prefer the *adj*-tautomer.[102,103] The repulsive transannular interactions of two protonated pyrroles (as well as the electrostatic repulsion of the two imine-type N-atoms) adjacent to each other are the major factors in the higher energies of the isobacteriochlorins compared to the corresponding bacteriochlorin isomers. The *adj*-tautomer was also observed as the preferred solution and solid-state structures for the isobacteriodilactones.[39]

An alternative tautomeric state of the isobacteriodilactones that alleviates the repulsive transannular interactions by protonating an oxazolone and a pyrrole on opposite sides of the macrocycle is also conceivable. In fact, this tautomer was, on the basis of iterative extended Hückel calculations, predicted by Gouterman et al. to be of the lowest energy.[36] Why, then, is a more strained tautomer observed experimentally for the isobacteriodilactones? Because tautomerization also impacts the favorability of the conjugation path through the nitrogen atoms,[104] how does the aromaticity of the macrocycle change as a function of the tautomeric state? The following analysis illuminates these questions.

We computed the *adj*- and *opp*-tautomers of the bacterio- and isobacteriodilactones and compared their energy (ΔE) relative to the lowest energy isomer/tautomer combination (***opp*-0E0∃**). We also computed NICS and macrocyclic current susceptibility strength (J_{macro}) values as complementary measures of aromaticity (Figure 4; for a full table of all results see the Supporting Information). NICS provides a measure of the magnetic shielding induced by the circulation of electron density in the molecule, whereas J_{macro} gives a measure of the ring current susceptibility for specific bonds or atoms. The use of both metrics reinforces our conclusions and provides a bridge to make comparisons with the literature data that may use only one or the other of these methodologies. The two tautomeric states of porphin were added as benchmark data.

Like others before us,[105] we found that the *adj*-tautomer of porphin is 8−9 kcal/mol less stable than the *opp*-tautomer. In addition, the analysis of the tautomers of porphin reveals that both possess essentially the same J_{macro} and NICS aromaticity metrics (of ∼27 nA/T and −38 ppm, respectively). The aromaticity of the two tautomers is thus independent of their thermodynamic stability. In turn, this suggests that the ΔE difference of the *opp*- versus *adj*-isomer is—at least at first approximation—of purely steric nature, induced by the repulsive transannular interactions within the central cavity of the *adj*-tautomer,[105] and not by any differences in their aromatic stabilization.

Similar transannular interactions in the central cavities of the porphodilactones destabilize any of the *adj*-isobacteriodilactones by 7−9 kcal/mol relative to the *opp*-bacteriodilactones. The aromaticity of the five experimentally observed

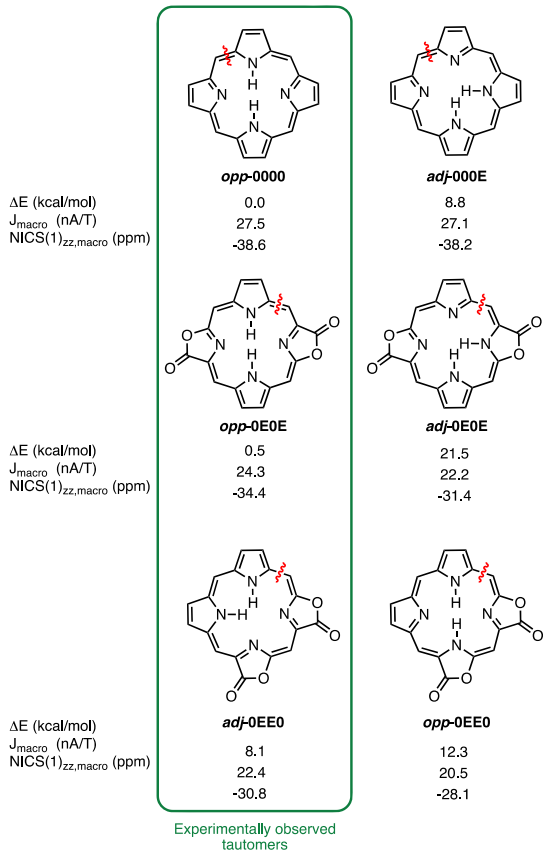

Figure 4. Relative energy (ΔE), absolute macrocyclic ring current susceptibility (J_{macro}), and absolute macrocyclic NICS ($NICS(1)_{ZZ,macro}$) for the compounds indicated. The ΔE of the porphyrins is listed relative to the *opp*-porphyrin shown, and ***opp*-0E0∃** in the dilactone series is set to be at ΔE = 0 kcal/mol. The red mark on each structure indicates the bond through the middle of which J_{macro} was integrated; $NICS(1)_{ZZ,macro}$ values were taken as the ZZ magnetic shielding component measured by a probe (phantom) atom 1 Å above the geometric mean of the $C_{12}N_4$ inner rim of each macrocycle.

porphodilactone isomers are within 10% of one another as quantified by J_{macro} (22.0−24.3 nA/T) and NICS (−30.2 to −34.4 ppm). Thus, as with porphin, the destabilization of the *adj*-isobacteriodilactones versus the *opp*-bacteriodilactones is primarily due to the unfavorable steric contacts within the central cavity of the macrocycle.

Considering the alternative tautomeric states of the porphodilactones, we find that the naturally occurring *adj*-isobacteriodilactones are by ∼3−4 kcal/mol stabilized over their hypothetical *opp*-tautomers; inversely, the *opp*-bacteriodilactones are stabilized by 19.4−22.0 kcal/mol over their hypothetical *adj*-tautomers. Part of the destabilization of *adj* versus *opp* bacteriodilactone tautomers is due to the introduction of unfavorable transannular repulsions, which we have just shown to inflict a 7−9 kcal/mol energetic penalty. If the destabilizing influences are assumed to be independent and additive to first order, some other factor destabilizes the *adj*-bacteriodilactones by an additional 12−13 (19−7 or 22−9) kcal/mol relative to the *opp* tautomers. This amount of destabilization is very nearly equal to that incurred (11−14 kcal/mol) by the isomerization of an *opp*-bacteriodilactone to an *opp*-isobacteriodilactone, which does not introduce any unfavorable transannular interactions.

DOI: 10.1021/acs.jpca.9b05656
J. Phys. Chem. A 2019, 123, 7470−7485

The canonical Lewis structures of the *adj*-bacteriodilactones and *opp*-isobacteriodilactones suggest the identity of an (additional) destabilizing factor: the protonated oxazolone found only in these isomer/tautomer combinations that formally imposes a break in the macrocyclic conjugation pathway. Surprisingly, however, the tautomers carrying a protonated oxazolone are, as measured by their corresponding J_{macro} values, only 10−20% less macrocycle-aromatic compared to the experimentally found tautomers. In other words, a protonated oxazolone can still sustain a significant ring current. To put this relatively small loss of macrocycle-aromaticity into perspective, the J_{macro} and NICS values of all five dilactones in their experimentally-observed tautomers are 10−20% smaller compared to those for porphin and, as noted above, they vary only within 10% from each other. Nonetheless, the reduction in aromaticity has a significant energetic effect, found here to be worth 11−14 kcal/mol.

In summary, steric strain (7−9 kcal/mol) in the *adj* and reduced aromaticity (11−14 kcal/mol) in the *opp*-tautomers destabilize the isobacteriodilactones relative to the *opp*-bacteriodilactones. Thus, the decrease in aromaticity for the *opp*-isobacteriodilactones is 3−4 kcal/mol more destabilizing than the repulsive interactions caused by adopting an *adj*-tautomer. By contrast, both steric strain and reduced aromaticity work in concert to destabilize the *adj*- versus *opp*-tautomers of the bacteriodilactones. The *adj*-bacteriodilactones are more strained (by 7−9 kcal/mol) and less aromatic (by 11−14 kcal/mol) than the *opp*-tautomers, which is in excellent agreement with the overall energy difference (19.4−22.0 kcal/mol) between these tautomers.

The interplay between the steric and electronic factors fully rationalizes the experimentally observed *opp*-bacteriodilactones and *adj*-isobacteriodilactones as the lowest energy porphodilactone tautomers[16,39] (this also extends to bacteriodilactone derivatives)[59] and corrects earlier predictions.[36] The outcome of this analysis is commensurate with the general observations made for porphyrins.[102,103] As the "unnatural" tautomers do not contribute to any significant degree to the equilibrium mixtures, they are not considered further in this report.

3.5. Interaction of the Oxazolones with the Macrocycle π-System: Aromaticity of the Porphodilactone Isomers. The energetic competition between steric and electronic factors that decides the tautomeric preference of a porphodilactone may suggest that thermodynamic stability and aromaticity are decoupled for these nonclassical hydroporphyrins. Such a conclusion would be in contrast to an investigation by Otero et al. for di-, tetra-, hexa- and octahydroporphyrins.[93] However, the transferability of conclusions for these structural classes to the porpholactones is not obvious because the latter vary in important aspects from their hydroporphyrin congeners. For example, the optical spectra of the porphodilactones do not resemble those of any type of classic hydroporphyrin.[10,106] The C_β-atom of each oxazolone is still sp^2-, instead of sp^3-hybridized, and is conjugated to an exocyclic π-bond (C═O). Also, the lone pairs of the β-oxa atoms, absent in the classic hydroporphyrins, are to some degree in conjugation with the macrocyclic π-system (for further details, see below). A change of the relative orientation of the two lactone moieties to each other results in different optical spectra,[16,39] suggesting a complex interaction of the lactone moieties with the macrocycle π-system or each other. The surprisingly strong influence of the relative orientation of auxochromes on the electronic properties of a porphyrinoid has been observed in other cases as well.[8,11,13,18,107] These effects are opposed to those caused by the removal of C_β═C_β bonds from crosstalk with the macrocycle by saturation in the classic hydroporphyrins.

To better understand the influence of the lactone moieties on the chromophore, we investigated the effects of the relative oxazolone orientation on the macrocycle aromaticity in all porphodilactone isomers and compared the results to the benchmark bacteriochlorin and isobacteriochlorin tetrahydroporphyrins (Table 2). Computed macrocyclic ring current susceptibilities and experimental ^{1}H NMR resonance data are used in the following discussion to assess the relative aromaticity of the porphodilactones.

Table 2. Calculated Macrocyclic Ring Current Susceptibilities (J_{macro}) and Experimental Proton Chemical Shifts for the Isomeric Dilactones and Reference Structures[a]

		experimental ^{1}H NMR resonances (ppm)[16,39]		
structure	calculated[a] macrocyclic current susceptibility (nA/T)	N−H protons	β-H protons	Δ (NH− to β-H proton resonance spread) (ppm)
0E0∃	23.2	−0.33, −0.95	8.52, 8.53, 8.70	8.9−9.7
0E0E	24.3	−2.12	8.85	10.8
0E∃0	22.0	−0.15	8.61, 8.71	8.8−8.9
0EE0	22.4	−0.32, −0.75	8.65, 8.68, 8.79	9.0−9.5
0∃E0	23.4	−1.99	8.83, 8.87	10.8−10.9
bacteriochlorin	23.5			
isobacteriochlorin	18.7			

[a]Based on a GIMIC analysis of NMR calculations at the B3LYP/def2TZVP level of theory.

The relative oxazolone orientation modulates the aromatic character of the porphodilactones over a narrow range: bacteriochlorin-type isomer **0E0E** is calculated to have a 1.1 nA/T greater macrocyclic ring current susceptibility than **0E0∃**.[108] The prediction is qualitatively in accord with the experimentally observed 1.2−1.8 ppm upfield and 0.15−0.33 ppm downfield shifts of the N−H and β-proton resonances, respectively, in the ^{1}H NMR spectrum of **0E0E** relative to that of **0E0∃**. Generally, the bacteriodilactones are, within ∼1.0 nA/T, just as aromatic as their unmodified hydroporphyrin congener.

The isobacteriodilactone isomer **0∃E0** is calculated to have a macrocyclic current susceptibility that is 1.4 nA/T greater than that of isomer **0E∃0**, whereas **0EE0** and **0E∃0** have very similar susceptibilities (within 0.4 nA/T). The experimental ^{1}H NMR shifts reflect this trend:[39] the N−H resonances of **0∃E0** are shifted upfield by at least 1.2 ppm relative to those of **0E∃0** and **0EE0**, which each show N−H signals in the −0.15 to −0.75 ppm range. The β-H resonances are correspondingly shifted downfield by 0.04−0.26 ppm. Notably, all isobacteriodilactones are by 3.3−4.7 nA/T significantly more aromatic than their tetrahydroporphyrin counterpart.

DOI: 10.1021/acs.jpca.9b05656
J. Phys. Chem. A 2019, 123, 7470−7485

Considering all five porphodilactones, the calculated diatropicity increases in the order **0E∃0** ≈ **0EE0** < **0∃E0** ≈ **0E0∃** < **0E0E**. The observed spread in the chemical shifts between the N−H and *β*-H resonances, an experimental measure of diatropicity, conforms to the same trend within, but not between, the sets of *adj*-isobacteriodilactone and *opp*-bacteriodilactone isomers. According to the experimental NMR data, **0E0∃** and **0EE0**, as well as **0E0E** and **0∃E0** form pairs of equivalently aromatic isomers. Neither the experimental nor computational diatropicity rankings of all five porphodilactones match the trend in their thermodynamic ground-state stability computationally derived in Section 3.4. This sets the dilactones apart from their tetrahydroporphyrin analogues.

The analysis of aromaticity was extended to visualize the magnetically induced currents in the bacteriodilactones and isobacteriodilactones using a streamline representation and quantified by numerically integrating the current flow through selected atoms and bonds (Figure 5). The general pattern that

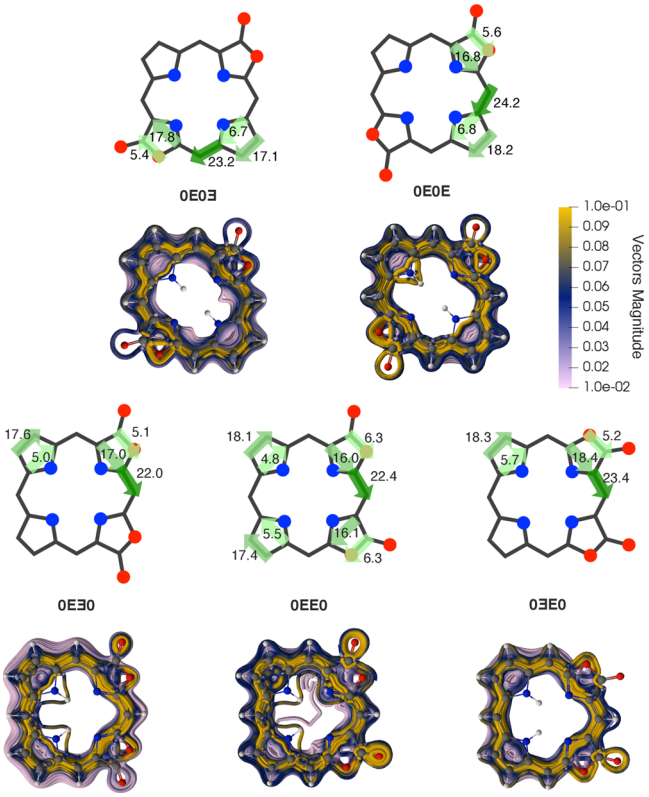

Figure 5. Ring currents in the porphodilactone isomers indicated with current susceptibilities in the units of nA/T integrated through symmetry unique atoms and bonds, and visualized below as streamlines using ParaView version 5.5.2.[109] For generating the streamlines, an inspection sphere with a radius of 0.8 Å was placed 1.0 Å below the same *meso*-carbon to provide a global view of the currents. The lavender-to-yellow color scale indicates an increasing amount of current.

emerges is that the macrocyclic current in all five porphodilactones primarily takes—as found for the conjugation pathways of the hydroporphyrins—the route through the outer C_β═C_β and the inner C_α−N−C_α bonds.[82] However, some current also flows through the C_α−NH−C_α units of the pyrroles, as found previously for a variety of porphyrinoids.[104] Significantly, and first demonstrated here, the lactone C_β−O_β bonds of the oxazolones also carry a sizable current, each sustaining a current susceptibility J_{macro} of 5.1−6.3 nA/T. However, the participation of the two C_β−O_β bonds leads only in the isobacteriodilactone cases to an increased J_{macro} relative to the corresponding hydroporphyrin (Table 2).

3.6. Detailed View on the Role of the Oxazolone Moieties. The calculated C_β−O_β bond current susceptibility suggests that the *β*,*β*′-bonds of a porphodilactone, unlike a classic hydroporphyrin, remain conjugated to the macrocycle. However, the current susceptibility is calculated by integrating through the middle of the C_β−O_β bond, meaning that the magnetically induced circulation of both *σ*- and *π*-electron densities is included. The close proximity of circulating nonbonding electrons of the (oxa and oxo) oxygen atoms to the integration plane used for the current density can also affect the results. To separate the macrocyclic conjugation from these other effects, we considered a model of an isolated 2,4-bis-C_{sp^2}-substituted oxazolone fragment to characterize its intrinsic properties apart from the macrocycle (Figure 6). The

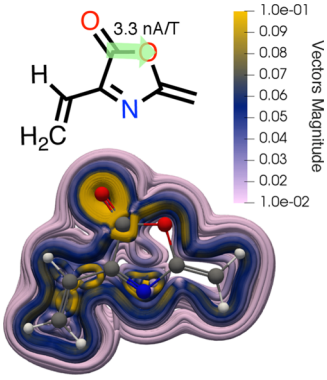

Figure 6. Oxazolone model system and depiction of local currents. An inspection sphere with a radius of 0.8 Å was placed 1.0 Å below the meso-position, so the streamlines are directly comparable to those in Figure 5.

computed current for the C_β−O_β bond in the oxazolone model system is 3.3 nA/T. This value is taken as the reference value in the absence of a macrocyclic current contribution. In comparison, the computed current susceptibility value for the C_β−O_β bond in the aromatic systems of the porphodilactones is significantly larger at 5.1−6.3 nA/T (Figure 5). This therefore indicates that ∼1.8−3.3 nA/T of the current susceptibility is due to conjugation of the oxazolone with the rest of the macrocycle. Previous studies similarly concluded on the basis of spectroscopic evidence and molecular orbital visualizations that the oxazolones were integrated into the electronic structure of the porpholactone chromophore.[15,16,37] However, the present study is the first to estimate the degree of conjugation of the lactone moiety with the macrocyclic *π*-system, and its influence on the aromaticity of the porphodilactones.

3.7. Reproduction of the Porphodilactone Optical Spectra. Having characterized the regioisomeric dependence of the ground-state thermodynamic stability and aromaticity among the porphodilactones, we next examined the modulation of their linear optical response properties. We thus computed the theoretical spectra resulting from TD-DFT vertical excitation energy calculations of all porphodilactone isomers (for details of the computations, see the Supporting Information). Relative to the spectrum of **0E00**,[37] the

DOI: 10.1021/acs.jpca.9b05656
J. Phys. Chem. A 2019, 123, 7470−7485

conversion of a second pyrrole into an oxazolone introduces a splitting of the Soret band and a significant modulation of the Q-bands in terms of band patterns and positions (Figure 7).

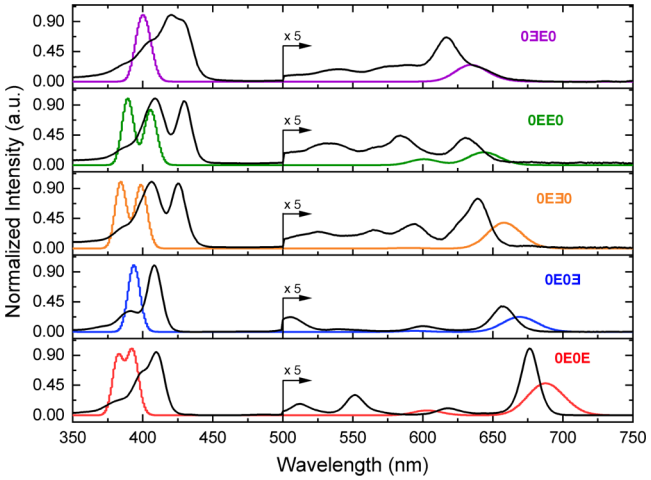

Figure 7. Experimental (black) and simulated (colored; vacuum-optimized structures, with the *meso*-C_6F_5 substituents replaced by hydrogen atoms) spectra for the compounds indicated. Gaussians with a full-width-at-half-maximum of 0.08 eV were fit to the calculated vertical excitation energies. A shift of 0.3637 eV was applied to all computed excitation energies because this is the discrepancy between theory and experiment for the parent porpholactone **0E00**, as explained in the Supporting Information. Both experimental and computational spectra were magnified five-fold for wavelengths beyond 500 nm for better visibility.

The overlay of the calculated results with the corresponding experimental absorption spectra highlights the high degree to which theory reproduces the key features of the experimental spectra: the overlapping or split Soret bands, their range, the features unique to some isomers, and the experimental Q-band wavelength trends among the porphodilactones. Of particular interest is the regioisomeric variation of the longest wavelength absorption over 52 nm, which is quantitatively reproduced by theory. Identifying the nature of this absorption band, and the origin of its modulation, is a chief objective of the following discussion.

3.8. Origin of the Porphodilactone Optical Spectra.

The visible absorption bands of porphyrins and hydroporphyrins are generally interpreted using the Gouterman four orbital model,[106] which considers the spectra as primarily originating from electronic transitions between the two highest occupied and two lowest unoccupied molecular orbitals. The origin of the optical spectra for the porphodilactone isomers are also well described by this model (Figure 8).

Figure 8 shows the energetic positions of the four frontier orbitals for the porphodilactone isomers arranged from left to right in order of the bathochromic shift in the longest wavelength absorption maximum. Ordinarily, bathochromic shifts of this kind are interpreted in terms of a narrowing of the HOMO−LUMO gap,[106] and indeed, this perspective explains the progressive red shift from **0EE0** to **0E0E**. In the sequence from **0EE0** rightward, the LUMO is stabilized and the LUMO +1 is destabilized, whereas the HOMO levels display much less variation.

In contrast to the general trend relating a reduced orbital gap to spectral bathochromism, the HOMO−LUMO separation increases from **0∃E0** to **0EE0**, even though the longest

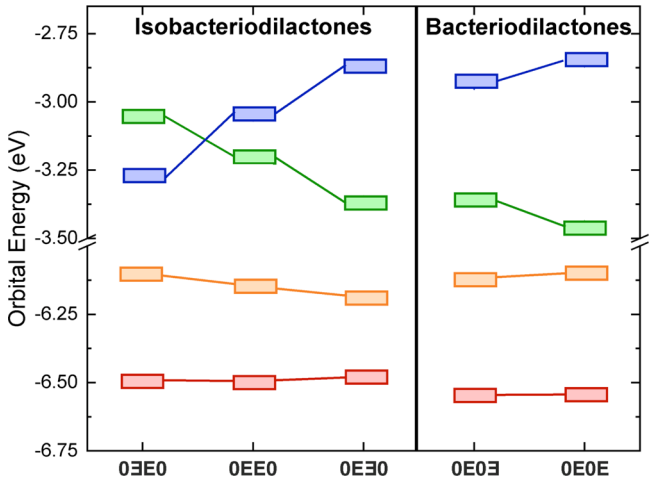

Figure 8. Frontier orbital energies for the five porphodilactone isomers. The coloring of the energy levels reflects similarities in the topology of the orbitals. Red, orange, green, and blue indicate respectively the HOMO − 1, HOMO, LUMO, and LUMO + 1, except for **0∃E0** for which the topologies of the LUMO and LUMO + 1 are inverted.

wavelength absorption red-shifts. This observation indicates that it is not sufficient to view the excitation in terms of a single electron promotion. Consistent with the four orbital model,[106] the excitation is shown below to be composed of multiple interacting electronic configurations. It is also interesting to note that, as we have previously shown,[39] the orbital topologies of the two LUMOs are inverted in isobacteriodilactone isomer **0∃E0** relative to those found for the other structures.

The calculations indicate that the longest wavelength (λ_{max}) band of the porphodilactones is composed of 63−76% HOMO → LUMO and 20−32% HOMO − 1 → LUMO + 1 orbital transitions. This spectral feature is therefore assigned as the Q_y state in accord with the four orbital model. The other low-lying and less intense electronic excitation in the Q-band region of the spectrum is dominated by HOMO − 1 → LUMO and HOMO → LUMO + 1 transitions and assigned as the Q_x state. Because the electronic structure calculations only found these two excited states in the long wavelength region (>500 nm), the additional band structure in the experimental spectra (Figure 7) is attributed to vibronic transitions. In the experimental spectra, it is difficult to distinguish the Q_x state from the Q-band vibronic progression. As is also the case for hydroporphyrins, the Q_y state in the porphodilactone isomers is generally lower in energy than the Q_x state, with the exception of isobacteriodilactone isomer **0∃E0**. The excitation wavelengths, oscillator strengths, and excited-state configurational compositions are tabulated for all five porphodilactone isomers in the Supporting Information.

The inverted state ordering for this isomer represents the culmination of a trend among the *adj*-isobacteriodilactones (see the Supporting Information for a full characterization of the Q_x and Q_y excited states): along the isomeric series **0E∃0** → **0EE0** → **0∃E0**, the Q_y−Q_x separation decreases and the relative intensities of these states significantly change, the two states mix configurationally, and ultimately the state ordering inverts. For **0E∃0**, the Q_y excitation is calculated to be 68 nm bathochromically shifted and 49-fold more intense relative to Q_x (oscillator strengths of 0.083 and 0.002 a.u., respectively). For isomer **0EE0**, by comparison, both the Q_y−Q_x wavelength

DOI: 10.1021/acs.jpca.9b05656
J. Phys. Chem. A 2019, 123, 7470−7485

separation and the Q_y intensity are nearly halved, the Q_x oscillator strength is more than an order of magnitude larger, and 8% of Q_x-native orbital transitions are mixed into the Q_y excitation (oscillator strengths 0.045 and 0.021 a.u., respectively). Isomerization to **0∃E0** blue-shifts the Q_y excitation 13 nm with respect to Q_x. The intensity of the Q_y state rebounds (to 0.079 a.u.), whereas Q_x retains a low oscillator strength (0.010 a.u.). The stabilization of Q_x below Q_y for **0∃E0** suggests that this isomer has an electronic structure more similar to a porphyrin than a hydroporphyrin. The different electronic structure of **0∃E0**, including the inverted unoccupied orbital ordering, significantly alters the dipolar properties of the molecule upon excitation into the Q_y state relative to the other isobacteriodilactones (see below).

3.9. Structure−Optical Property Correlations. With the experimental absorption spectra well reproduced by theory (Section 3.7) and the electronic structures of the porphodilactones characterized (Section 3.8), we now seek to disclose the structural origins for the Q_y-band wavelength modulation of the isomers. This regioisomer effect has begun to be discussed in the literature[59] and was shown to have had a number of important practical consequences.[16,110,111] We hypothesized that the spectral modulation of the Q_y-band has an electrostatic origin (Table 3), whereby the bathochromic trend results from the lactone moieties preferentially stabilizing the ground-state and/or destabilizing the excited-state electron distribution. Recall that the Q_y wavelength red-shifts in the order **0∃E0** < **0EE0** < **0E∃0** < **0E0∃** < **0E0E**. The ground and Q_y excited states are increasingly stabilized along the isobacteriodilactone series, but stabilization in the corresponding excited-state energies is 1.6−2.6-fold larger (Table 3). Thus, the bathochromic shift among the isobacteriodilactones is the result of a preferential excited-state stabilization. By contrast, the ground and Q_y excited states of bacteriodilactone **0E0E** are destabilized and stabilized, respectively, to equal extents relative to those for **0E0∃**. The bathochromic shift among the bacteriodilactones, therefore, is the result of the equal and opposing energetic changes to both the ground and excited states.

Table 3. Relative Energies of the Ground (ΔE_{gs}) and Excited States (ΔE_{es}), Absolute Dipole Moments, and Q_y λ_{max} Wavelengths for the Porphodilactone Isomers[a]

	ΔE_{gs}[b]	$\lvert\mu_{gs}\rvert$	ΔE_{es}[b]	$\lvert\mu_{es}\rvert$	calc (nm)	exp (nm)
0∃E0	9.1	10.68	62.7	11.58	630	624
0EE0	7.7	9.77	60.5	9.02	640	631
0E∃0	7.1	8.80	58.9	8.85	654	640
0E0∃	0.0	2.12	51.1	1.22	665	657
0E0E	0.6	0.00	50.5	0.00	683	676

[a]All quantities were calculated at the PBE0[71]/6-31+G(d) level of theory, the same model used for the excited state calculations. [b]All energies are relative to the ground state of **0E0∃**, set to be 0.0.

The relative orientation of the oxazolone moieties strongly influences the dipolar properties of the macrocycle. The increased stability in the ground state for most, and excited state for all, isomers correlates with a decreased polarity in the respective states. The correlation may reflect the energetic favorability of a molecule of lower polarity in a low dielectric environment (vacuum of the calculations or the CH_2Cl_2 solvent used experimentally). With regard to the spectral trend, the ranking of isomers by the Q_y-band red-shift linearly correlates with a decreasing magnitude of the ground and Q_y excited-state molecular dipole moments. The Q_y band red-shifts as the oxazolone carbonyl bond dipoles become increasingly antiparallel. However, computations of compounds in which the lactone carbonyl groups (C═O) were formally replaced by methylene groups (C═CH_2) could not confirm a connection between the position of the Q_y λ_{max} band and the overall polarity of the chromophore (for details, see the Supporting Information).

What, then, is the structural origin of the red-shifts in the Q_y band among the five porphodilactone isomers? What are the minimal structural requirements needed to realize the pronounced differences between the regioisomers? In addressing these questions, we performed two series of calculations: starting with monolactone **0E00**, we formally exchanged a second pyrrole C_β═C_β bond by a number of nonsymmetric moieties and we computed the corresponding Q_y bands for all regioisomers (Figure 9A,B). We restricted the replacement options to carba-analogues of the oxazolone moiety, that is, O═C−CH_2, H_2C═C−CH_2, H_2C═C−O, and so forth. The search was furthermore limited to five-membered rings because the expansion of the ring introduces significant conformational effects that, in turn, alter the optical spectra in a major way.[29,32,112] This substitution series allowed the delineation of Q_y-band wavelength variation in terms of the following influences: (1) cross-conjugation of an exocyclic π-bond in the absence of any oxygen atoms, (2) an exocyclic sp^2- or sp^3-hybridized oxygen atom, and (3) an sp^3-hybridized oxygen atom either directly connected to an sp^2-hybridized carbon of the macrocyclic chromophore or an intervening sp^3-hybridized C_β atom. We monitored two aspects of the spectral modulation under these structural perturbations, namely, the absolute position of the Q_y band and the difference between the isomers within each structural series (isobacterio- and bacteriochlorin-type isomers).

An inspection of the spectral outcomes of the modifications in the bacteriochlorin series (Figure 9A) reveals that the presence of the lactone moiety (oxazolone building block) results, together with the pyrrole building block, in the most blue-shifted derivative. A differentiation of the two isomers that is similar to the experimental 19 nm split between the porphodilactones **0E0E** versus **0E0∃** can only be observed when a ring oxa-atom or a ring-oxo-substituent is present, whereby the effects of the two structural features are not additive. The oxo- and oxa-components of the lactone moiety exert opposing influences. A replacement of the electron-withdrawing oxo-group by a more electron-rich methylene group results in an almost 100 nm bathochromic shift, whereas the carba-analogues of the oxa-derivatives are significantly blue-shifted. Comparison of some of the previously reported bisoxazolobacteriochlorins prepared by us with closely related carba-analogues prepared by Lindsey and co-workers provided already some experimental precedent for this effect.[56,113−118]

These findings are principally also found for the isobacteriochlorin series (Figure 9B), with the complication of the presence of three isomers per compound, and the fact that the trends are not exactly the same for each isomer. It is nonetheless possible to make some general observations. The globally more blue-shifted optical spectra of the isobacteriochlorins versus the spectra of the corresponding bacteriochlorin analogues is preserved for all substitutions. Analogous to the bacteriochlorin series, the isobacteriochlorin derivatives carrying a pyrrole- and oxazolone-building block represent the

DOI: 10.1021/acs.jpca.9b05656
J. Phys. Chem. A 2019, 123, 7470−7485

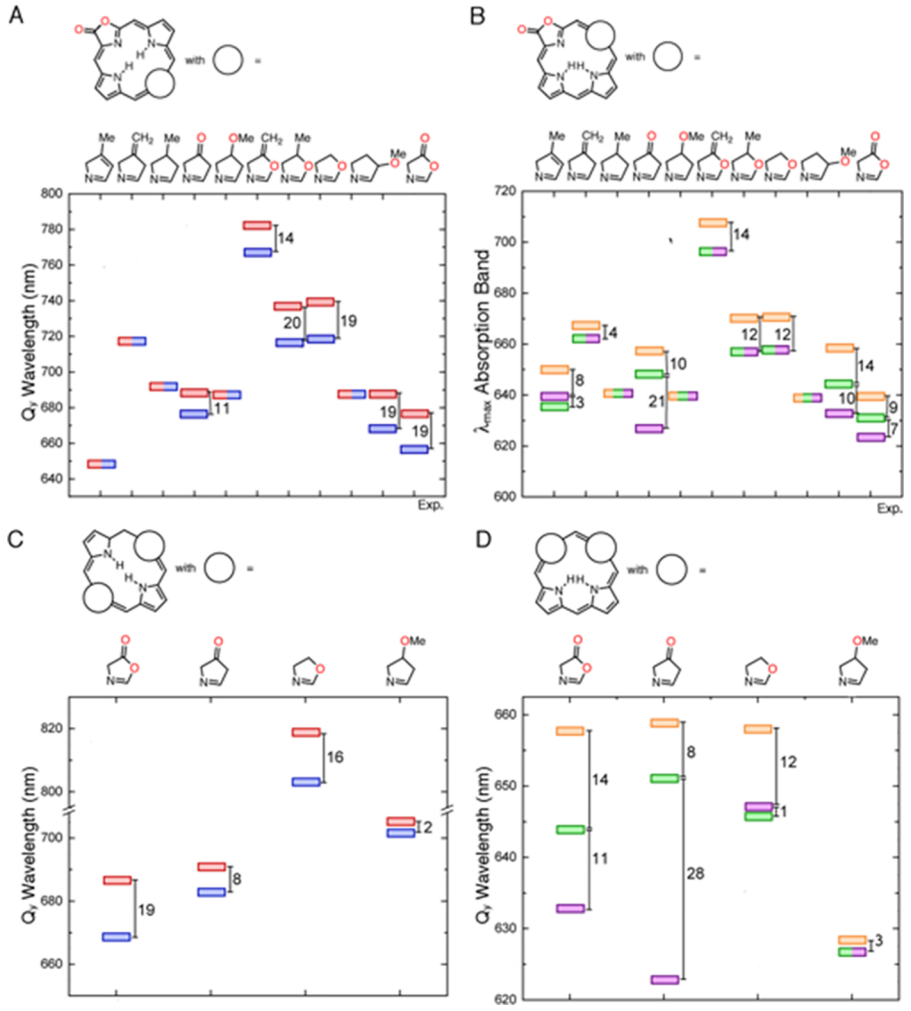

Figure 9. Structural substitution pattern for the (A) *opp*-bacteriodilactones and (B) *adj*-isobacteriodilactones in which a C_β═C_β bond of a second pyrrole in monolactone **0E00** was replaced by nonsymmetric functionalities. Structural substitution pattern for the (C) *opp*-bacteriodilactone and (D) *adj*-isobacteriodilactone derivatives in which both O═C_β–O_β moieties were replaced by the same nonsymmetric functionality. All simulated excitation energies were obtained at the PBE0/6-31+G(d) level of theory and uniformly shifted by 0.3637 eV to lower energy. The longest wavelength absorption is shown for each analogue. For an analysis of the electronic configurations of these absorptions and their assignment as Q_y or Q_x, see the Supporting Information. In all parts, purple, green, orange, blue, and red indicate **0∃E0**, **0EE0**, **0E∃0**, **0E0∃**, and **0E0E**, or structural analogues with the same regiochemistry as these compounds.

compounds with the most blue-shifted spectra. Inversely, the methylene-analogue (H_2C═C–O) to the oxazolone is most red-shifted. The analogues in which the oxa- or oxo-atoms, or both, are replaced by a methylene completely retain, partially preserve, or completely lose the regioisomeric differentiation of their λ_{max} band positions. The terms "completely" and "partially" refer to the presence, respectively, of wavelength differences among all three or only two of the isobacteriochlorin-type isomers, and not to the magnitudes of these differences.

In a second series of calculations, we formally replaced both lactone (O═C–O) moieties of the porphodilactone isomers with the same nonsymmetric moiety chosen from among those examined above and we calculated the Q_y bands for all regioisomers (Figure 9C,D). This procedure allowed the definition of the minimal structural features that are needed to realize isomer-dependent Q_y-wavelength variations within the bacteriochlorin- and isobacteriochlorin-type series. The wavelength differences between the regioisomers are essentially lost in the all-carbon ring derivative CH_3O–CH–CH_2 (Figure 9C,D). Only if the building blocks possess oxygen atoms bonded to an sp^2-hybridized C_α and C_β position as a ring oxa-atom or a C_β-oxo-substituent is a strong electronic effect exerted on the chromophore, as expressed in Q_y band shifts or large differences between regioisomers. The following section will further illuminate to which degree these types of oxygens are in conjugation with the macrocycle π-system.

3.10. Role of the Lactone Oxa- and Oxo-Atoms. A natural bond orbital (NBO) analysis for the five porphodilactone isomers (presented in the Supporting Information) identified partial delocalization of a nonbonding electron pair into the porphyrinic π-system as the unique interaction shared by the oxo- or oxa-oxygen atoms; neither a CH_2 nor a CH–OCH_3 moiety could provide a corresponding interaction. However, the NBO analysis showed no meaningful variation in the degree of lone-pair delocalization between the porphodilactone isomers. It thus is only suited to explain the absolute wavelength shifts observed for derivatives with and without these interacting oxygen atoms, but not the isomeric differences within each structural family.

DOI: 10.1021/acs.jpca.9b05656
J. Phys. Chem. A 2019, 123, 7470–7485

To rationalize the isomeric differences within the bacterio- and isobacteriochlorin-type isomers, we hypothesized that the relative orientation of these lactone groups significantly alters the charge shift upon excitation. To test this conjecture, we calculated the change in electron density (excited state−ground state) for all regioisomers of structures with either two O═C−CH_2 moieties (large computed optical difference between the isomers) or CH_3O−CH−CH_2 (negligible computed optical difference between the isomers) moieties (cf. Figures 9 and 10). Analogous charge shift plots for the five porphodilactones are given in the Supporting Information.

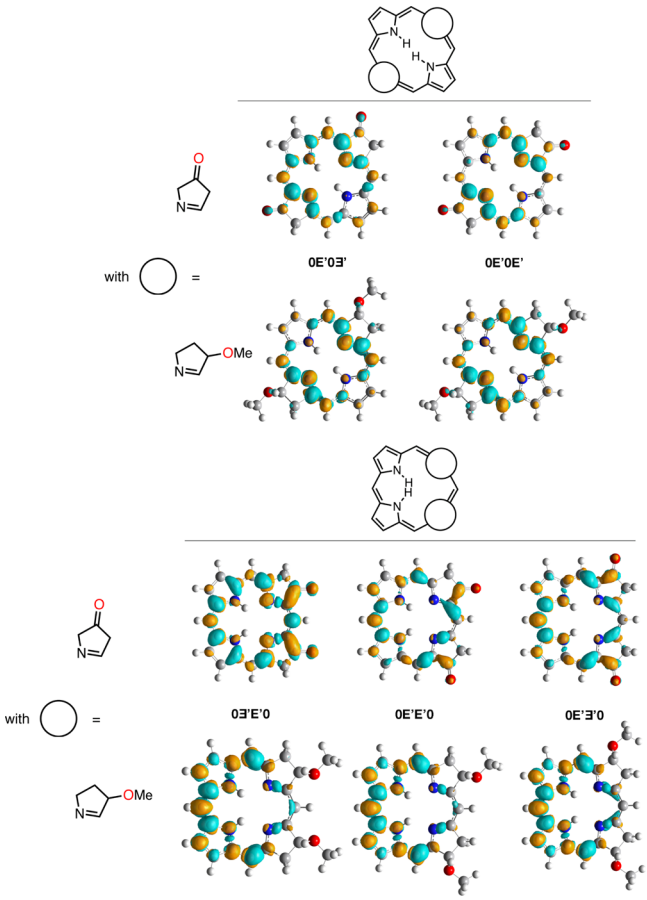

Figure 10. Difference density plots for the excitation of bacteriochlorin- and isobacteriochlorin-type analogues of the corresponding porphodilactones. Lobes indicate regions that change electron density upon excitation: orange—gain, blue—loss. The densities are shown at an isovalue of 5×10^{-3} a.u.

Upon excitation into the Q_y state for both classes of bacteriochlorin-type structures shown, there is an alternating pattern of gain and loss of electron density over the inner rim of C_{meso}-, C_α-, and N-atoms and some accumulation of density on the conjugated C_β-positions. However, when considering the differences between the β-keto and β-methoxy-substituted derivatives, we note that the extended macrocycle π-conjugation involving the β-oxo oxygens significantly alters the charge shift within the pyrrole building blocks; it also introduces significant electron reorganization differences in their regioisomeric derivatives. For instance, either isomer of the β-methoxy-substituted bacteriochlorin-type analogue (**0E′0E′** and **0E′0∃′**) shows loss and gain of electron density on both C_α- and both C_β-atoms of the pyrroles. By contrast, the diketo analogues either show a decrease and increase of charge density, respectively, on only one C_α-atom and one C_β-atom of each pyrrole (**0E′0E′**), or on the C_α- and C_β-atoms of different pyrroles (**0E′0∃′**). Thus, the conjugation of the β-oxygen substituents is needed to polarize the charge shift upon excitation in a regioisomeric-dependent fashion. In the context of oxygen lone-pair delocalization, it is also noteworthy that there is loss—albeit small at the chosen isovalue—of electron density from the keto (but not the methoxy) oxygens, and gain on the carbonyl carbons in both isomers upon excitation.

Similar conclusions follow for the isobacteriochlorin-type diketo- and dimethoxy-substituted regioisomers. The three methoxy-bearing isomers all have charge shifts and Q_y wavelengths that are practically identical, whereas the diketo-substituted counterparts exhibit significant changes in the excitation-induced electron reorganization throughout the macrocycle. Electron density flows in an oxazolone-to-pyrrole direction in isomers **0E′E′0** and **0E′∃0′**, whereas in the opposite direction in **0∃′E′0** as a consequence of the inverted energetic ordering of the unoccupied orbitals..

4. CONCLUSIONS

In summary, we delineated the relationships between structure and thermodynamic stability, aromaticity, and optical properties for all regioisomers of the porphodilactones. The two bacteriodilactone-type isomers adopt an *opp*-tautomeric state to minimize strain and maximize aromaticity, whereas the three isobacteriodilactone-type isomers occur as *adj*-tautomers to maximize aromaticity at the price of increased strain. The competition between the steric and electronic factors produces different trends in thermodynamic stability and aromaticity, setting the porphodilactones apart from their classic hydroporphyrin congeners. The porphodilactones are furthermore differentiated by the fact that the oxazolone C_β−O_β bond has a degree of conjugation with the macrocycle that lies in-between that of a HC═CH and H_2C−CH_2 bond, explaining why in some cases the porpholactones are porphyrin-like, and in others chlorin-like. Based on magnetic criteria, all five porphodilactones possess levels of aromaticity that are within 10% of one another and ≥80% of that found for porphin. The Q_y wavelength for all isomers is experimentally tuned over a 52 nm range. Conjugation of β-oxygen atoms on opposite (bacteriochlorin-type substituent pattern) or adjacent sites (isobacteriochlorin-type substituent pattern) of the macrocycle was found to be the minimal structural requirement for a regioisomeric tuning of the optical properties. The conjugated oxygens partially delocalize nonbonding electrons into the macrocycle and polarize the charge shifts upon excitation, but they do so in a regioisomer-dependent fashion. In that respect, we can confirm the findings by Shen, Sessler, and Zhang,[59] but we cannot support their generalization of the regioisomeric effects; they are expected to be observed in only specialized cases. Likewise, we cannot find a correlation between aromaticity and regioisomeric electronic differences in our narrowly defined set of chromophores and attribute their finding to their particular choice of chromophores.

These mechanistic insights into the electronic structure of the regioisomeric porphodilactones provide a structural basis for the versatile and precise modulation of porphyrinoid optical properties by systematically varying the number, nature, relative orientation, and degree of conjugation of β-substituents. The porphodilactone analogues theoretically considered in this work constitute only a small subset of the

DOI: 10.1021/acs.jpca.9b05656
J. Phys. Chem. A 2019, 123, 7470−7485

chemical space that awaits experimental exploration along these lines.[10−13] The work will inform the design and utilization of pyrrole-modified porphyrins for a range of biomedical and technical applications.

■ ASSOCIATED CONTENT

Supporting Information

The Supporting Information is available free of charge on the ACS Publications website at DOI: 10.1021/acs.jpca.9b05656.

meso-Aryl group rotational itineraries for the bacteriodilactones; a tabulation of relative energies, NICS, and macrocyclic ring current susceptibilities for all considered isomer/tautomer combinations; computational details for excited states, details on the suspected Q_y wavelength−molecular dipole moment correlation; an oxazolone-centered NBO analysis, and optimized coordinates for the five porphodilactone isomers with *meso*-hydrogens (PDF)

■ AUTHOR INFORMATION

Corresponding Authors

*E-mail: matthew.guberman-pfeffer@uconn.edu (M.J.G.-P.).
*E-mail: jose.gascon@uconn.edu (J.A.G.).

ORCID

Christian Brückner: 0000-0002-1560-7345
José A. Gascón: 0000-0002-4176-9030

Notes

The authors declare no competing financial interest.

■ ACKNOWLEDGMENTS

This work was supported by the US National Science Foundation under grant numbers DGE-1247393 (to M.J.G.-P.), CHE-1465133 and CHE-1800361 (to C.B.), and CHE-0754580 (to J.A.G.). We thank Jun-Long Zhang, Peking University, for the experimental spectra of the bacteriodilactones. We thank Heike Fliegl for her assistance with how to implement the GIMIC method.

■ REFERENCES

(1) Agius, L.; Ballantine, J. A.; Ferrito, V.; Jaccarini, V.; Murray-Rust, P.; Pelter, A.; Psaila, A. F.; Schembri, P. J. The structure and physiological activity of bonellin - a unique chlorin derived from Bonellia viridis. *Pure Appl. Chem.* **1979**, *51*, 1847−1864.

(2) Pettit, G. R.; Kantoci, D.; Doubek, D. L.; Tucker, B. E.; Pettit, W. E.; Schroll, R. M. Isolation of the nickel-chlorin chelate tunichlorin from the South Pacific ocean sea hare Dolabella auricularia. *J. Nat. Prod.* **1993**, *56*, 1981−1984.

(3) Bible, K. C.; Buytendorp, M.; Zierath, P. D.; Rinehart, K. L. Tunichlorin: A nickel chlorin isolated from the Caribbean tunicate Tridemnum solidum. *Proc. Natl. Acad. Sci. U.S.A.* **1988**, *85*, 4582−4586.

(4) Rinehart, K. L.; Kishore, V.; Bible, K. C.; Sakai, R.; Sullins, D. W.; Li, K.-M. Didemnins and tunichlorin-novel natural-products from the marine tunicate Tridemnum solidum. *J. Nat. Prod.* **1988**, *51*, 1−21.

(5) Murphy, M. J.; Siegel, L. M.; Tove, S. R.; Kamin, H. Siroheme: A new prosthetic group participating in six-electron reduction reactions catalyzed by both sulfite and nitrite reductases. *Proc. Natl. Acad. Sci. U.S.A.* **1974**, *71*, 612−616.

(6) Chiu, J. T.; Loewen, P. C.; Switala, J.; Gennis, R. B.; Timkovich, R. Proposed structure for the prosthetic group of the catalase HpII from Escherichia coli. *J. Am. Chem. Soc.* **1989**, *111*, 7046−7050.

(7) Scheer, H. The Pigments. *Light-Harvesting Antennas in Photosynthesis*; Springer, 2003; pp 29−81.

(8) Chen, M. Chlorophyll modifications and their spectral extension in oxygenic photosynthesis. *Annu. Rev. Biochem.* **2014**, *83*, 317−340.

(9) Shelnutt, J. A.; Song, X.-Z.; Ma, J.-G.; Jentzen, W.; Medforth, C. J. Nonplanar porphyrins and their significance in proteins. *Chem. Soc. Rev.* **1998**, *27*, 31−41.

(10) Brückner, C.; Samankumara, L.; Ogikubo, J. Syntheses of Bacteriochlorins and Isobacteriochlorins. In *Handbook of Porphyrin Science*; Kadish, K. M., Smith, K. M., Guilard, R., Eds.; World Scientific: River Edge, NY, 2012; Vol. *17*, pp 1−112.

(11) Lindsey, J. S. De novo synthesis of gem-dialkyl chlorophyll analogues for probing and emulating our green world. *Chem. Rev.* **2015**, *115*, 6534−6620.

(12) Borbas, K. E. Chlorins. *Handbook of Porphyrin Science*; World Scientific Publishing Company, 2016; Vol. *36*, pp 1−149.

(13) Taniguchi, M.; Lindsey, J. S. Synthetic chlorins, possible surrogates for chlorophylls, prepared by derivatization of porphyrins. *Chem. Rev.* **2017**, *117*, 344−535.

(14) Schwabe, T. Review of proteinochromism modeling in computational chemistry. *Curr. Org. Chem.* **2017**, *21*, 856−871.

(15) Brückner, C.; McCarthy, J. R.; Daniell, H. W.; Pendon, Z. D.; Ilagan, R. P.; Francis, T. M.; Ren, L.; Birge, R. R.; Frank, H. A. A spectroscopic and computational study of the singlet and triplet excited states of synthetic β-functionalized chlorins. *Chem. Phys.* **2003**, *294*, 285−303.

(16) Ke, X.-S.; Chang, Y.; Chen, J.-Z.; Tian, J.; Mack, J.; Cheng, X.; Shen, Z.; Zhang, J.-L. Porphodilactones as synthetic chlorophylls: Relative orientation of β-substituents on a pyrrolic ring tunes NIR absorption. *J. Am. Chem. Soc.* **2014**, *136*, 9598−9607.

(17) Chang, C. K. On the structure of heme d_1. An isobacteriochlorin derivative as the prosthetic group of dissimilatory nitrite reductase. *J. Biol. Chem.* **1985**, *260*, 9520−9522.

(18) Chang, C. K.; Barkigia, K. M.; Hanson, L. K.; Fajer, J. Models of heme d_1. Structure and redox chemistry of dioxoisobacteriochlorins. *J. Am. Chem. Soc.* **1986**, *108*, 1352−1354.

(19) Barkigia, K. M.; Chang, C. K.; Fajer, J.; Renner, M. W. Models of heme d_1. Molecular structure and NMR characterization of an iron(III) dioxoisobacteriochlorin (porphyrindione). *J. Am. Chem. Soc.* **1992**, *114*, 1701−1707.

(20) Romanowski, F.; Mai, G.; Kusch, D.; Montforts, F.-P.; Bats, J. W. Stereoselektive Synthese des Nitrit-reduzierenden Cofaktors Häm d1ausgehend von Hämatoporphyrin. *Helv. Chim. Acta* **1996**, *79*, 1572−1586.

(21) Prinsep, M. R.; Caplan, F. R.; Moore, R. E.; Patterson, G. M. L.; Smith, C. D. Tolyporphin, a novel multidrug resistance reversing agent from the blue-green alga Tolypothrix nodosa. *J. Am. Chem. Soc.* **1992**, *114*, 385−387.

(22) Prinsep, M. R.; Patterson, G. M. L.; Larsen, L. K.; Smith, C. D. Further tolyporphins from the blue-green alga Tolypothrix nodosa. *Tetrahedron* **1995**, *51*, 10523−10530.

(23) Prinsep, M. R.; Patterson, G. M. L.; Larsen, L. K.; Smith, C. D. Tolyporphins J and K, two further porphinoid metabolites from the cyanobacterium Tolypothrix nodosa. *J. Nat. Prod.* **1998**, *61*, 1133−1136.

(24) Wang, W.; Kishi, Y. Synthesis and structure of tolyporphin a O,O-diacetate. *Org. Lett.* **1999**, *1*, 1129−1132.

(25) Hood, D.; Niedzwiedzki, D. M.; Zhang, R.; Zhang, Y.; Dai, J.; Miller, E. S.; Bocian, D. F.; Williams, P. G.; Lindsey, J. S.; Holten, D. Photophysical characterization of tolyporphin A, a naturally occurring dioxobacteriochlorin, and synthetic oxobacteriochlorin analogues. *Photochem. Photobiol.* **2017**, *93*, 1204−1215.

(26) Barnhart-Dailey, M.; Zhang, Y.; Zhang, R.; Anthony, S. M.; Aaron, J. S.; Miller, E. S.; Lindsey, J. S.; Timlin, J. A. Cellular localization of tolyporphins, unusual tetrapyrroles, in a microbial photosynthetic community determined using hyperspectral confocal fluorescence microscopy. *Photosynth. Res.* **2019**, DOI: 10.1007/s11120-019-00625-w.

(27) Flitsch, W. *Hydrogenated Porphyrin Derivatives: Hydroporphyrins*; Advances in Heterocyclic Chemistry; Academic Press, 1988; Vol. *43*, pp 73−126.

DOI: 10.1021/acs.jpca.9b05656
J. Phys. Chem. A 2019, 123, 7470−7485

(28) Montforts, F.-P.; Gerlach, B.; Hoeper, F. Discovery and synthesis of less common natural hydroporphyrins. *Chem. Rev.* **1994**, *94*, 327−347.
(29) Brückner, C. The breaking and mending of meso-tetraarylporphyrins: Transmuting the pyrrolic building blocks. *Acc. Chem. Res.* **2016**, *49*, 1080−1092.
(30) Arnold, L.; Müllen, K. Modifying the porphyrin core - a chemist's jigsaw. *J. Porphyrins Phthalocyanines* **2011**, *15*, 757−779.
(31) Lash, T. D. Carbaporphyrins, porphyrin isomers and the legacy of Emanuel Vogel. *J. Porphyrins Phthalocyanines* **2012**, *16*, 423−433.
(32) Brückner, C.; Akhigbe, J.; Samankumara, L. Syntheses and structures of porphyrin analogues containing non-pyrrolic heterocycles. In *Handbook of Porphyrin Science*; Kadish, K. M., Smith, K. M., Guilard, R., Eds.; World Scientific: River Edge, NY, 2014; Vol. *31*, pp 1−276.
(33) Szyszko, B.; Latos-Grażyński, L. Core chemistry and skeletal rearrangements of porphyrinoids and metalloporphyrinoids. *Chem. Soc. Rev.* **2015**, *44*, 3588−3616.
(34) Costa, L.; Costa, J.; Tomé, A. Porphyrin macrocycle modification: Pyrrole ring-contracted or -expanded porphyrinoids. *Molecules* **2016**, *21*, 320.
(35) Crossley, M. J.; King, L. G. Novel heterocyclic systems from selective oxidation at the β-pyrrolic position of porphyrins. *J. Chem. Soc., Chem. Commun.* **1984**, 920−922.
(36) Gouterman, M.; Hall, R. J.; Khalil, G. E.; Martin, P. C.; Shankland, E. G.; Cerny, R. L. Tetrakis(pentafluorophenyl)-porpholactone. *J. Am. Chem. Soc.* **1989**, *111*, 3702−3707.
(37) Brückner, C.; Ogikubo, J.; McCarthy, J. R.; Akhigbe, J.; Hyland, M. A.; Daddario, P.; Worlinsky, J. L.; Zeller, M.; Engle, J. T.; Ziegler, C. J.; et al. meso-Arylporpholactones and their reduction products. *J. Org. Chem.* **2012**, *77*, 6480−6494.
(38) Yu, Y.; Lv, H.; Ke, X.; Yang, B.; Zhang, J.-L. Ruthenium-Catalyzed Oxidation of the Porphyrin β,β′-Pyrrolic Ring: A General and Efficient Approach to Porpholactones. *Adv. Synth. Catal.* **2012**, *354*, 3509−3516.
(39) Hewage, N.; Daddario, P.; Lau, K. S. F.; Guberman-Pfeffer, M. J.; Gascón, J. A.; Zeller, M.; Lee, C. O.; Khalil, G. E.; Gouterman, M.; Brückner, C. Bacterio- and isobacteriodilactones by stepwise or direct oxidations of meso-tetrakis(pentafluorophenyl)porphyrin. *J. Org. Chem.* **2019**, *84*, 239−256.
(40) Jayaraj, K.; Gold, A.; Austin, R. N.; Ball, L. M.; Terner, J.; Mandon, D.; Weiss, R.; Fischer, J.; DeCian, A.; Bill, E.; et al. Compound I and compound II analogues from porpholactones. *Inorg. Chem.* **1997**, *36*, 4555−4566.
(41) Yu, Y.; Furuyama, T.; Tang, J.; Wu, Z.-Y.; Chen, J.-Z.; Kobayashi, N.; Zhang, J.-L. Stable iso-bacteriochlorin mimics from porpholactone: effect of a β-oxazolone moiety on the frontier π-molecular orbitals. *Inorg. Chem. Front.* **2015**, *2*, 671−677.
(42) Liang, L.; Lv, H.; Yu, Y.; Wang, P.; Zhang, J.-L. Iron(III) tetrakis(pentafluorophenyl)porpholactone catalyzes nitrogen atom transfer to C=C and C-H bonds with organic azides. *Dalton Trans.* **2012**, *41*, 1457−1460.
(43) Rahimi, R.; Tehrani, A. A.; Fard, M. A.; Sadegh, B. M. M.; Khavasi, H. R. First catalytic application of metal complexes of porpholactone and dihydroxychlorin in the sulfoxidation reaction. *Catal. Commun.* **2009**, *11*, 232−235.
(44) Çetin, A.; Ziegler, C. J. Structure and catalytic activity of a manganese(III) tetraphenylporpholactone. *Dalton Trans.* **2005**, 25−26.
(45) To, W.-P.; Liu, Y.; Lau, T.-C.; Che, C.-M. A robust palladium(II)−porphyrin complex as catalyst for visible light induced oxidative C−H functionalization. *Chem.—Eur. J.* **2013**, *19*, 5654−5664.
(46) Wu, Z.-Y.; Wang, T.; Meng, Y.-S.; Rao, Y.; Wang, B.-W.; Zheng, J.; Gao, S.; Zhang, J.-L. Enhancing the reactivity of nickel(II) in hydrogen evolution reactions (HERS) by β-hydrogenation of porphyrinoid ligands. *Chem. Sci.* **2017**, *8*, 5953−5961.
(47) Ke, X.-S.; Yang, B.-Y.; Cheng, X.; Chan, S. L.-F.; Zhang, J.-L. Ytterbium(III) porpholactones: β−Lactonization of porphyrin ligands enhances sensitization efficiency of lanthanide near-infrared luminescence. *Chem.—Eur. J.* **2014**, *20*, 4324−4333.
(48) Gouterman, M.; Callis, J.; Dalton, L.; Khalil, G.; Mébarki, Y.; Cooper, K. R.; Grenier, M. Dual luminophor pressure-sensitive paint: III. Application to automotive model testing. *Meas. Sci. Technol.* **2004**, *15*, 1986−1994.
(49) Khalil, G. E.; Costin, C.; Crafton, J.; Jones, G.; Grenoble, S.; Gouterman, M.; Callis, J. B.; Dalton, L. R. Dual-luminophor pressure-sensitive paint. *Sens. Actuators, B* **2004**, *97*, 13−21.
(50) Zelelow, B.; Khalil, G. E.; Phelan, G.; Carlson, B.; Gouterman, M.; Callis, J. B.; Dalton, L. R. Dual luminophor pressure sensitive paint. *Sens. Actuators, B* **2003**, *96*, 304−314.
(51) Tang, J.; Chen, J.-J.; Jing, J.; Chen, J.-Z.; Lv, H.; Yu, Y.; Xu, P.; Zhang, J.-L. β-Lactonization of fluorinated porphyrin enhances LDL binding affinity, cellular uptake with selective intracellular localization. *Chem. Sci.* **2014**, *5*, 558−566.
(52) Khalil, G. E.; Daddario, P.; Lau, K. S. F.; Imtiaz, S.; King, M.; Gouterman, M.; Sidelev, A.; Puran, N.; Ghandehari, M.; Brückner, C. meso-Tetraarylporpholactones as high pH sensors. *Analyst* **2010**, *135*, 2125−2131.
(53) Worlinsky, J. L.; Halepas, S.; Brückner, C. PEGylated meso-arylporpholactone metal complexes as optical cyanide sensors in water. *Org. Biomol. Chem.* **2014**, *12*, 3991−4001.
(54) Liu, E.; Ghandehari, M.; Brückner, C.; Khalil, G.; Worlinsky, J.; Jin, W.; Sidelev, A.; Hyland, M. A. Mapping high pH levels in hydrated calcium silicates. *Cem. Concr. Res.* **2017**, *95*, 232−239.
(55) Ogikubo, J.; Brückner, C. Tunable meso-tetraphenylalkyloxazolo-chlorins and -bacteriochlorins. *Org. Lett.* **2011**, *13*, 2380−2383.
(56) Ogikubo, J.; Meehan, E.; Engle, J. T.; Ziegler, C. J.; Brückner, C. Oxazolochlorins. 9.meso-Tetraphenyl-2-oxabacteriochlorins and-meso-Tetraphenyl-2,12/13-dioxabacteriochlorins. *J. Org. Chem.* **2013**, *78*, 2840−2852.
(57) Rhoda, H. M.; Akhigbe, J.; Ogikubo, J.; Sabin, J. R.; Ziegler, C. J.; Brückner, C.; Nemykin, V. N. Magnetic circular dichroism spectroscopy of meso-tetraphenylporphyrin-derived hydroporphyrins and pyrrole-modified porphyrins. *J. Phys. Chem. A* **2016**, *120*, 5805−5815.
(58) Ning, Y.; Liu, Y.-W.; Meng, Y.-S.; Zhang, J.-L. Design of near-infrared luminescent lanthanide complexes sensitive to environmental stimulus through rationally tuning the secondary coordination sphere. *Inorg. Chem.* **2018**, *57*, 1332−1341.
(59) Yao, Y.; Rao, Y.; Liu, Y.; Jiang, L.; Xiong, J.; Fan, Y.-J.; Shen, Z.; Sessler, J. L.; Zhang, J.-L. Aromaticity versus regioisomeric effect of β-substituents in porphyrinoids. *Phys. Chem. Chem. Phys.* **2019**, *21*, 10152−10162.
(60) Becke, A. D. Density-functional thermochemistry. III. The role of exact exchange. *J. Chem. Phys.* **1993**, *98*, 5648−5652.
(61) Stephens, P. J.; Devlin, F. J.; Chabalowski, C. F.; Frisch, M. J. Ab initio calculation of vibrational absorption and circular dichroism spectra using density functional force fields. *J. Phys. Chem.* **1994**, *98*, 11623−11627.
(62) Grimme, S.; Antony, J.; Ehrlich, S.; Krieg, H. A consistent and accurate ab initio parametrization of density functional dispersion correction (DFT-D) for the 94 elements H-Pu. *J. Chem. Phys.* **2010**, *132*, 154104.
(63) King, R. A.; Crawford, T. D.; Stanton, J. F.; Schaefer, H. F. Conformations of [10]annulene: More bad news for density functional theory and second-order perturbation theory. *J. Am. Chem. Soc.* **1999**, *121*, 10788−10793.
(64) Wannere, C. S.; Sattelmeyer, K. W.; Schaefer, H. F., III; Schleyer, P. v. R. Aromaticity: The alternating C−C bond length structures of [14]-, [18]-, and [22]annulene. *Angew. Chem., Int. Ed.* **2004**, *43*, 4200−4206.
(65) Castro, C.; Chen, Z.; Wannere, C. S.; Jiao, H.; Karney, W. L.; Mauksch, M.; Puchta, R.; Hommes, N. J. R. v. E.; Schleyer, P. v. R. Investigation of a putative Möbius aromatic hydrocarbon. The effect of benzannelation on Möbius [4n]annulene aromaticity. *J. Am. Chem. Soc.* **2005**, *127*, 2425−2432.

DOI: 10.1021/acs.jpca.9b05656
J. Phys. Chem. A 2019, 123, 7470−7485

(66) Marcos, E.; Anglada, J. M.; Torrent-Sucarrat, M. Theoretical study of the switching between Hückel and Möbius topologies for expanded porphyrins. *J. Phys. Chem. C* **2012**, *116*, 24358−24366.
(67) Torrent-Sucarrat, M.; Navarro, S.; Cossío, F. P.; Anglada, J. M.; Luis, J. M. Relevance of the DFT method to study expanded porphyrins with different topologies. *J. Comput. Chem.* **2017**, *38*, 2819−2828.
(68) Valiev, R. R.; Fliegl, H.; Sundholm, D. Bicycloaromaticity and Baird-type bicycloaromaticity of dithienothiophene-bridged [34]-octaphyrins. *Phys. Chem. Chem. Phys.* **2018**, *20*, 17705−17713.
(69) Zhao, Y.; Truhlar, D. G. The M06 suite of density functionals for main group thermochemistry, thermochemical kinetics, noncovalent interactions, excited states, and transition elements: Two new functionals and systematic testing of four M06-class functionals and 12 other functionals. *Theor. Chem. Acc.* **2008**, *120*, 215−241.
(70) Yanai, T.; Tew, D. P.; Handy, N. C. A new hybrid exchange-correlation functional using the Coulomb-attenuating method (CAM-B3LYP). *Chem. Phys. Lett.* **2004**, *393*, 51−57.
(71) Adamo, C.; Barone, V. Toward reliable density functional methods without adjustable parameters: The PBE0 model. *J. Chem. Phys.* **1999**, *110*, 6158−6170.
(72) Barone, V.; Cossi, M. Quantum calculation of molecular energies and energy gradients in solution by a conductor solvent model. *J. Phys. Chem. A* **1998**, *102*, 1995−2001.
(73) Cossi, M.; Rega, N.; Scalmani, G.; Barone, V. Energies, structures, and electronic properties of molecules in solution with the C-PCM solvation model. *J. Comput. Chem.* **2003**, *24*, 669−681.
(74) Adamo, C.; Jacquemin, D. The calculations of excited-state properties with time-dependent density functional theory. *Chem. Soc. Rev.* **2013**, *42*, 845−856.
(75) London, F. Théorie quantique des courants interatomiques dans les combinaisons aromatiques. *J. Phys. Radium* **1937**, *8*, 397−409.
(76) Reid, R. V., Jr Nuclear magnetic shielding in the hydrogen molecule. *Phys. Rev. A: At., Mol., Opt. Phys.* **1975**, *11*, 403−408.
(77) Ditchfield, R. Self-consistent perturbation theory of diamagnetism. *Mol. Phys.* **1974**, *27*, 789−807.
(78) Wolinski, K.; Hinton, J. F.; Pulay, P. Efficient implementation of the gauge-independent atomic orbital method for NMR chemical shift calculations. *J. Am. Chem. Soc.* **1990**, *112*, 8251−8260.
(79) Weigend, F.; Ahlrichs, R. Balanced basis sets of split valence, triple zeta valence and quadruple zeta valence quality for H to Rn: Design and assessment of accuracy. *Phys. Chem. Chem. Phys.* **2005**, *7*, 3297−3305.
(80) Jusélius, J.; Sundholm, D.; Gauss, J. Calculation of current densities using gauge-including atomic orbitals. *J. Chem. Phys.* **2004**, *121*, 3952−3963.
(81) Taubert, S.; Sundholm, D.; Jusélius, J. Calculation of spin-current densities using gauge-including atomic orbitals. *J. Chem. Phys.* **2011**, *134*, 054123.
(82) Fliegl, H.; Sundholm, D. Aromatic pathways of porphins, chlorins, and bacteriochlorins. *J. Org. Chem.* **2012**, *77*, 3408−3414.
(83) Sancho-García, J. C.; Cornil, J. Assessment of recently developed exchange-correlation functionals for the description of torsion potentials in π-conjugated molecules. *J. Chem. Phys.* **2004**, *121*, 3096−3101.
(84) Refaely-Abramson, S.; Baer, R.; Kronik, L. Fundamental and excitation gaps in molecules of relevance for organic photovoltaics from an optimally tuned range-separated hybrid functional. *Phys. Rev. B: Condens. Matter Mater. Phys.* **2011**, *84*, 075144.
(85) Casademont-Reig, I.; Woller, T.; Contreras-García, J.; Alonso, M.; Torrent-Sucarrat, M.; Matito, E. New electron delocalization tools to describe the aromaticity in porphyrinoids. *Phys. Chem. Chem. Phys.* **2018**, *20*, 2787−2796.
(86) Chen, Z.; Wannere, C. S.; Corminboeuf, C.; Puchta, R.; Schleyer, P. V. R. Nucleus-independent chemical shifts (NICS) as an aromaticity criterion. *Chem. Rev.* **2005**, *105*, 3842−3888.
(87) Fallah-Bagher-Shaidaei, H.; Wannere, C. S.; Corminboeuf, C.; Puchta, R.; Schleyer, P. v. R. Which NICS aromaticity index for planar π rings is best? *Org. Lett.* **2006**, *8*, 863−866.
(88) Frisch, M. J.; Trucks, G. W.; Schlegel, H. B.; Scuseria, G. E.; Robb, M. A.; Cheeseman, J. R.; Scalmani, G.; Barone, V.; Mennucci, B.; Petersson, G. A.; et al. *Gaussian 09*, Revision D. 01; Gaussian. Inc.: Wallingford CT, USA, 2013.
(89) Moss, G. P. IUPAC-IUB Joint Commission on Biochemical Nomenclature, Nomenclature of tetrapyrroles. *Pure Appl. Chem.* **1987**, *59*, 779−832.
(90) Yoshida, K.; Osuka, A. Subporpholactone, subporpholactam, imidazolosubporphyrin, and iridium complexes of imidazolosubporphyrin: Formation of iridium carbene complexes. *Angew. Chem., Int. Ed.* **2018**, *57*, 338−342.
(91) Yu, Y.; Czepukojc, B.; Jacob, C.; Jiang, Y.; Zeller, M.; Brückner, C.; Zhang, J.-L. Porphothionolactones: Synthesis, structure, physical, and chemical properties of a chemidosimeter for hypochlorite. *Org. Biomol. Chem.* **2013**, *11*, 4613−4621.
(92) Brückner, C.; Foss, P. C. D.; Sullivan, J. O.; Pelto, R.; Zeller, M.; Birge, R. R.; Crundwell, G. Origin of the bathochromically shifted optical spectra of meso-tetrathien-2′- and 3′-ylporphyrins as compared to meso-tetraphenylporphyrin. *Phys. Chem. Chem. Phys.* **2006**, *8*, 2402−2412.
(93) Otero, N.; Fias, S.; Radenković, S.; Bultinck, P.; Graña, A. M.; Mandado, M. How does aromaticity rule the thermodynamic stability of hydroporphyrins? *Chem.—Eur. J.* **2011**, *17*, 3274−3286.
(94) Eaton, S. S.; Eaton, G. R. Kinetic isotope effect on proton tautomerism in tetraarylporphyrins. *J. Am. Chem. Soc.* **1977**, *99*, 1601−1604.
(95) Crossley, M. J.; Harding, M. M.; Sternhell, S. Tautomerism in 2-substituted 5,10,15,20-tetraphenylporphyrins. *J. Am. Chem. Soc.* **1986**, *108*, 3608−3613.
(96) Crossley, M. J.; Harding, M. M.; Sternhell, S. Tautomerism in 2-hydroxy-5,10,15,20-tetraphenylporphyrin: An equilibrium between enol, keto, and aromatic hydroxyl tautomers. *J. Org. Chem.* **1988**, *53*, 1132−1137.
(97) Crossley, M. J.; Harding, M. M.; Sternhell, S. Direct observation of tautomeric forms of deuteroporphyrin derivatives by proton NMR spectroscopy: Substituent effects and structure implications. *J. Org. Chem.* **1992**, *57*, 1833−1837.
(98) Barkigia, K. M.; Renner, M. W.; Xie, H.; Smith, K. M.; Fajer, J. Structural consequences of porphyrin tautomerization. Molecular structure of a zinc isoporphyrin. *J. Am. Chem. Soc.* **1993**, *115*, 7894−7895.
(99) Braun, J.; Koecher, M.; Schlabach, M.; Wehrle, B.; Limbach, H.-H.; Vogel, E. NMR study of the tautomerism of porphyrin including the kinetic HH/HD/DD isotope effects in the liquid and the solid state. *J. Am. Chem. Soc.* **1994**, *116*, 6593−6604.
(100) Wu, Y.-D.; Chan, K. W. K.; Yip, C.-P.; Vogel, E.; Plattner, D. A.; Houk, K. N. Porphyrin isomers: Geometry, tautomerism, geometrical isomerism, and stability. *J. Org. Chem.* **1997**, *62*, 9240−9250.
(101) Helaja, J.; Montforts, F.-P.; Kilpeläinen, I.; Hynninen, P. H. NH tautomerism in the dimethyl ester of bonellin, a natural chlorin. *J. Org. Chem.* **1999**, *64*, 432−437.
(102) Stepien, M.; Latos-Grazynski, L. *Aromaticity and Tautomerism in Porphyrins and Porphyrinoids*; Topics in Heterocyclic Chemistry; Springer, 2009; Vol. *19*, pp 83−153.
(103) Helaja, J.; Stapelbroek-Möllmann, M.; Kilpeläinen, I.; Hynninen, P. H. NH tautomerism in the natural chlorin derivatives. *J. Org. Chem.* **2000**, *65*, 3700−3707.
(104) Fliegl, H.; Valiev, R. R.; Pichierri, F.; Sundholm, D. M. B. Theoretical Studies as a Tool for Understanding the Aromatic Character of Porphyrinoid Compounds. *Chemical Modelling*; Royal Society of Chemistry, 2018; Vol. *14*, pp 1−42.
(105) AbuSalim, D. I.; Lash, T. D. In pursuit of novel porphyrin isomers. Aromatic character and relative stability of conjugated tetrapyrroles with two neo-confused rings or with mixed neo-confused and N-confused subunits. *J. Phys. Chem. A* **2015**, *119*, 11440−11453.

DOI: 10.1021/acs.jpca.9b05656
J. Phys. Chem. A 2019, 123, 7470−7485

(106) Gouterman, M. Optical Spectra and Electronic Structure of Porphyrins and Related Rings. In *The Porphyrins*; Dolphin, D., Ed.; Academic Press: New York, 1978; Vol. 3, pp 1−165.
(107) Inhoffen, H. H.; Nolte, W. Zur weiteren Kenntnis des Chlorophylls und des Hämins, XXIV1) Oxidative Umlagerungen am Octaäthylporphin zu Geminiporphin-polyketonen. *Justus Liebigs Ann. Chem.* **1969**, *725*, 167−176.
(108) The numerical error for these calculations is estimated to be (0.7 nA/T), and constant for all the studied structures. This estimate is based on Kirchhoff's circuit law that states that the sum of the current through all the branches in a circuit must be equal to the total current. The sum of the currents through the C−NH−C and C−C or C−O paths of any subunit are within 0.7 nÅ/T of the current flowing through a C_{α}−C_{meso} bond. This value is thus taken as the minimal relative numerical error from one structure to another.
(109) Ayachit, U. *The ParaView Guide: A Parallel Visualization Application*; Kitware, 2015, ISBN 978-1930934306.
(110) Ke, X.-S.; Zhao, H.; Zou, X.; Ning, Y.; Cheng, X.; Su, H.; Zhang, J.-L. Fine-Tuning of *β*-Substitution to Modulate the Lowest Triplet Excited States: A Bioinspired Approach to Design Phosphorescent Metalloporphyrinoids. *J. Am. Chem. Soc.* **2015**, *137*, 10745−10752.
(111) Ke, X.-S.; Ning, Y.; Tang, J.; Hu, J.-Y.; Yin, H.-Y.; Wang, G.-X.; Yang, Z.-S.; Jie, J.; Liu, K.; Meng, Z.-S.; et al. Gadolinium(III) porpholactones as efficient and robust singlet oxygen photosensitizers. *Chem.—Eur. J.* **2016**, *22*, 9676−9686.
(112) Guberman-Pfeffer, M. J.; Greco, J. A.; Samankumara, L. P.; Zeller, M.; Birge, R. R.; Gascón, J. A.; Brückner, C. Bacteriochlorins with a twist: Discovery of a unique mechanism to red-shift the optical spectra of bacteriochlorins. *J. Am. Chem. Soc.* **2017**, *139*, 548−560.
(113) Liu, M.; Chen, C.-Y.; Hood, D.; Taniguchi, M.; Diers, J. R.; Bocian, D. F.; Holten, D.; Lindsey, J. S. Synthesis, photophysics and electronic structure of oxobacteriochlorins. *New J. Chem.* **2017**, *41*, 3732−3744.
(114) Zhang, S.; Kim, H.-J.; Tang, Q.; Yang, E.; Bocian, D. F.; Holten, D.; Lindsey, J. S. Synthesis and photophysical characteristics of 2,3,12,13-tetraalkylbacteriochlorins. *New J. Chem.* **2016**, *40*, 5942−5956.
(115) Mandal, A. K.; Sahin, T.; Liu, M.; Lindsey, J. S.; Bocian, D. F.; Holten, D. Photophysical comparisons of PEGylated porphyrins, chlorins and bacteriochlorins in water. *New J. Chem.* **2016**, *40*, 9648−9656.
(116) Liu, Y.; Lindsey, J. S. Northern-Southern route to synthetic bacteriochlorins. *J. Org. Chem.* **2016**, *81*, 11882−11897.
(117) Vairaprakash, P.; Yang, E.; Sahin, T.; Taniguchi, M.; Krayer, M.; Diers, J. R.; Wang, A.; Niedzwiedzki, D. M.; Kirmaier, C.; Lindsey, J. S.; et al. Extending the short and long wavelength limits of bacteriochlorin near-infrared absorption via dioxo- and bisimide-functionalization. *J. Phys. Chem. B* **2015**, *119*, 4382−4395.
(118) Jiang, J.; Taniguchi, M.; Lindsey, J. S. Near-infrared tunable bacteriochlorins equipped for bioorthogonal labeling. *New J. Chem.* **2015**, *39*, 4534−4550.

DOI: 10.1021/acs.jpca.9b05656
J. Phys. Chem. A 2019, 123, 7470−7485